



# Planetary fertility during the past 400 ka based on the triple isotope composition of O<sub>2</sub> in trapped gases from the Vostok ice core

T. Blunier<sup>1</sup>, M. L. Bender<sup>2</sup>, B. Barnett<sup>2,\*</sup>, and J. C. von Fischer<sup>2,3</sup>

<sup>1</sup>Centre for Ice and Climate, Niels Bohr Institute, University of Copenhagen, Juliane Maries Vej 30, 2100 Copenhagen Ø, Denmark

<sup>2</sup>Department of Geosciences, Princeton University, Guyot Hall, Princeton, NJ 08544, USA

<sup>3</sup>Department of Biology, Colorado State University, Ft. Collins, CO 80523, USA

\*now at: Nicholas School of the Environment, Duke University, Durham, NC 27708, USA

Correspondence to: T. Blunier (blunier@gfy.ku.dk)

Received: 2 January 2012 – Published in Clim. Past Discuss.: 30 January 2012

Revised: 15 August 2012 – Accepted: 25 August 2012 – Published: 10 October 2012

**Abstract.** The productivity of the biosphere leaves its imprint on the isotopic composition of atmospheric oxygen. Ultimately, atmospheric oxygen, through photosynthesis, originates from seawater. Fractionations during the passage from seawater to atmospheric O<sub>2</sub> and during respiration affect  $\delta^{17}\text{O}$  approximately half as much as  $\delta^{18}\text{O}$ . An “anomalous” (also termed mass independent) fractionation process changes  $\delta^{17}\text{O}$  about 1.7 times as much as  $\delta^{18}\text{O}$  during isotope exchange between O<sub>2</sub> and CO<sub>2</sub> in the stratosphere. The relative rates of biological O<sub>2</sub> production and stratospheric processing determine the relationship between  $\delta^{17}\text{O}$  and  $\delta^{18}\text{O}$  of O<sub>2</sub> in the atmosphere. Variations of this relationship thus allow us to estimate changes in the rate of O<sub>2</sub> production by photosynthesis versus the rate of O<sub>2</sub>–CO<sub>2</sub> isotope exchange in the stratosphere. However, the analysis of the <sup>17</sup>O anomaly is complicated because each hydrological and biological process fractionates  $\delta^{17}\text{O}$  and  $\delta^{18}\text{O}$  in slightly different proportions. In this study we present O<sub>2</sub> isotope data covering the last 400 ka (thousand years) from the Vostok ice core. We reconstruct oxygen productivities from the triple isotope composition of atmospheric oxygen with a box model. Our steady state model for the oxygen cycle takes into account fractionation during photosynthesis and respiration by the land and ocean biosphere, fractionation during the hydrologic cycle, and fractionation when oxygen passes through the stratosphere. We consider changes of fractionation factors linked to climate variations, taking into account the span of estimates of the main factors affecting our calculations. We find that ocean oxygen productivity was within 20 % of the mod-

ern value throughout the last 400 ka. Given the presumed reduction in terrestrial oxygen productivity, the total oxygen production during glacials was likely reduced.

## 1 Introduction

Understanding the interaction between climate and the biosphere is of interest for a number of reasons. First, climate obviously plays a fundamental role in determining properties of terrestrial and marine ecosystems. Second, properties of the biosphere have a significant influence on climate. In the terrestrial realm, the biosphere plays a basic role in the hydrologic cycle and also influences climate via its impact on albedo. In the marine realm, biologically mediated carbon fluxes affect the partial pressure of CO<sub>2</sub> in the surface ocean and hence the atmospheric burden of this gas. Ocean and terrestrial biogeochemical processes are also significant sources to the atmosphere of, e.g., N<sub>2</sub>O and halocarbons (see, e.g. Hirsch et al., 2006; Smythe-Wright et al., 2006, and references therein).

Most studies of the past biosphere involve the examination of local ecosystems. Examples pertaining to the Pleistocene include pollen studies of land ecosystems and sedimentary proxy measures of the past fertility of ocean ecosystems (e.g. Kohfeld et al., 2005). On the other hand, measurements of the isotopic composition of O<sub>2</sub> in air provide a means to access the fertility of ocean and land ecosystems at the global scale (Luz et al., 1999; Blunier et al., 2002; Landais et al.,

2007). The global rate of photosynthesis is encoded in the magnitude of the mass-independent signal of  $O_2$  in air. A series of photochemical reactions in the stratosphere, mediated by  $O_3$  and  $O(^1D)$ , lead to isotope exchange between  $O_2$  and  $CO_2$ . In this exchange, the heavy isotope abundance of  $CO_2$  rises and that of  $O_2$  falls. Unlike “normal” reactions, in which  $\delta^{17}O$  is fractionated nominally 0.5 times as much as  $\delta^{18}O$ , the stratospheric  $O_2$ – $CO_2$  exchange fractionates  $\delta^{17}O$  1.7 times as much as  $\delta^{18}O$  (Thiemens et al., 1995; Boering et al., 2004; Lämmerzahl et al., 2002). This stratospheric fractionation is said to be “anomalous”, or “mass independent”. Consequently, the  $\delta^{17}O$  of  $O_2$  in air is less than that of  $0.5 \cdot \delta^{18}O$ . The magnitude of this anomaly depends on the rate of photosynthesis and respiration by the biosphere. Respiration consumes ambient  $O_2$ , with its stratospheric anomaly, and photosynthesis replaces it with  $O_2$  produced from water, which is normally fractionated. Photosynthesis and respiration thus attenuate the magnitude of the mass independent anomaly in the triple isotope composition of atmospheric  $O_2$ . To a first approximation, the magnitude of the anomaly scales linearly with the  $CO_2$  concentration of air (which promotes exchange), and inversely with the fertility of the planet (Luz et al., 1999). With data on the atmospheric  $CO_2$  concentration and the mass independent fractionation of  $O_2$ , one can calculate the total rate of photosynthesis and respiration on Earth. There are important complications to this calculation (Blunier et al., 2002; Landais et al., 2007), and these are discussed below.

The productivity thus determined is the total rate of  $O_2$  production by the ocean and land biospheres. Of greater interest is the past productivity within each of these realms. In principle, one can partition total production based on the  $\delta^{18}O$  of  $O_2$  in air. The  $\delta^{18}O$  of leaf water is enriched by evapotranspiration relative to seawater, causing  $O_2$  from land photosynthesis to be enriched in  $^{18}O$  relative to  $O_2$  from ocean photosynthesis.  $\delta^{18}O$  of  $O_2$  in air thus reflects the relative rates of terrestrial and marine photosynthesis, allowing us to partition total production between land and oceans. We adopt this approach here but note that, in practice, confounding factors introduce large uncertainties, and we need to allow for these uncertainties in interpreting our results.

In this paper, we first present data that extends the 65 ka record of the mass-independent fractionation of  $O_2$  in air (Blunier et al., 2002) through the full 400 ka length of the Vostok ice core record, with approximately 1 ka resolution. We next outline the background for interpreting the data, in general following the approach outlined above and the formalism of Blunier et al. (2002), brought up to date with results from recent important experiments. We then focus on the implications of our results for the fertility of the global biosphere. We emphasize the ocean biosphere because the terrestrial biosphere is arguably somewhat better constrained with pollen data, at least at the Last Glacial Maximum.

## 2 Experiment

Samples were analyzed using the method first described by Luz et al. (1999) and modified by Blunier et al. (2002). Trapped gases were extracted from approximately 70 g of ice by inserting ice into a  $\sim 500 \text{ cm}^3$  Pyrex vessel sealed with an Ace Threads connector and a shaft-seal elastomer valve (Louwers-Hapert). The flask was chilled to about  $-70^\circ\text{C}$  and evacuated. The flask was then allowed to warm to room temperature and air was extracted using the method of Emerson et al. (1995). In this method, the water is equilibrated with the headspace by rotating the flask for several hours. The flask is inverted and most of the water is removed by vacuum. The flask is again righted, cooled to  $-40^\circ\text{C}$  in a chilled propanol bath, and noncondensibles frozen through a water trap at  $-70^\circ\text{C}$  onto mole sieve at liquid nitrogen temperature. The gas sample is then chromatographed to separate other gases from  $O_2$  and Ar;  $O_2$  is analyzed for  $\delta^{17}O$  and  $\delta^{18}O$  of  $O_2$  by triple collector isotope ratio mass spectrometry (Finnigan MAT 252). Corrections are made for residual  $N_2$  in the sample and reference gases, to which the measured values of  $\delta^{18}O$  and especially  $\delta^{17}O$  are very sensitive. The  $O_2/Ar$  ratios are very close to atmospheric values.

The  $\delta^{17}O$  and  $\delta^{18}O$  ratios are normalized to atmospheric  $O_2$ , used here as the standard, based on frequent analyses of air. The data are reported as  $^{17}\Delta$  with respect to modern air. Following Miller (2002), and Luz and Barkan (2005),  $^{17}\Delta$  is defined as:

$$^{17}\Delta \equiv \ln(\delta^{17}O + 1) - \lambda_{\text{ref}} \cdot \ln(\delta^{18}O + 1) \quad (1)$$

The coefficient,  $\lambda_{\text{ref}}$  is 0.516. It is an approximation for the exact ratio of  $^{17}O/^{18}O$  fractionation during processes influencing the isotopic composition of  $O_2$  in modern air (Luz and Barkan, 2005). Equation (1) may be approximated linearly as  $\Delta^{17}O = \delta^{17}O - \lambda_{\text{ref}} \cdot \delta^{18}O$  (Luz et al., 1999), and we used this definition in our previous publication (Blunier et al., 2002).

Equation (1) is a definition, and it works best when  $\lambda_{\text{ref}}$  is selected to account for the primary process leading to isotope fractionation, which in our case is mitochondrial respiration. The optimal value for the coefficient also depends on whether that process is best characterized as Rayleigh distillation (irreversible, closed-system transformation) or steady-state. For a Rayleigh process (fractionation of water isotopes in the hydrologic cycle), the coefficient is equal to  $\gamma = (^{17}\alpha - 1)/(^{18}\alpha - 1)$ . For a steady-state process (atmospheric  $O_2$  cycle, in which photosynthesis is continuously balanced by respiration), the coefficient equals  $\lambda = \ln(^{17}\alpha)/\ln(^{18}\alpha)$  (Blunier et al., 2002).

As indicated above, the fractionation ratio ( $^{17}\alpha/^{18}\alpha$ ) varies among different mass-dependent processes. Consequently,  $^{17}\Delta$  of  $O_2$  will deviate slightly from zero even in the absence of mass-independent processes. In the case of atmospheric  $O_2$ , mass-dependent effects contribute significantly to deviations from zero  $^{17}\Delta$  and their variations with time (Blunier

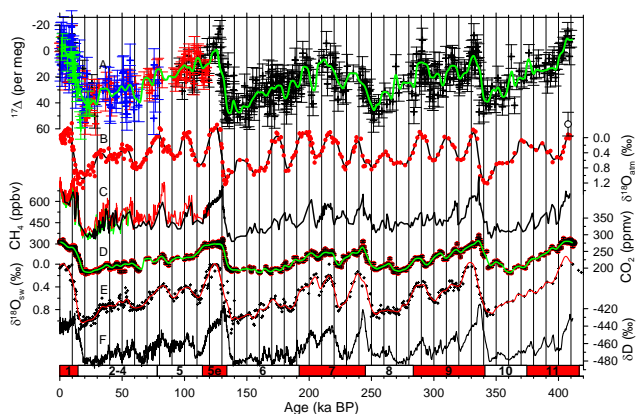


**Fig. 1.** (A)  $^{17}\Delta$  from the Vostok, GISP2, GISP2 and Siple Dome cores (Blunier et al., 2002) represented as black, red, blue, and green crosses, respectively. (B)  $\delta^{18}\text{O}$  in paleoatmospheric  $\text{O}_2$  from Vostok (Petit et al., 1999). (C)  $\text{CH}_4$  data from Vostok, GISP2 and Siple Dome, respectively in similar colors as the  $^{17}\Delta$  data (see text for references and details). (D) Compiled  $\text{CO}_2$  data from Vostok, Taylor Dome and EPICA Dome C (see text for details and references). (E)  $\delta^{18}\text{O}$  of seawater from Shackleton (2000). (F)  $\delta\text{D}$  record from Vostok (Petit et al., 1999). The underlying time scale for the study is the orbitally tuned Vostok time scale from Suwa and Bender (2008).

et al., 2002; Landais et al., 2006; Miller, 2002). We discuss this issue below.

### 3 Results

A total of 555 samples from 317 depth levels were analyzed from the Vostok ice core. Additionally, 196 samples from 80 depth levels were measured on the GISP2 core. Generally samples were analyzed in duplicate. The original data from Blunier et al. (2002) from the GISP2 and the Siple Dome cores were converted from the  $\Delta^{17}\text{O}$  scale to the  $^{17}\Delta$  scale. The data are shown in per meg (1 per meg = 0.001 ‰) in Fig. 1, with standard errors for the mean calculated from the pooled standard deviation for replicate samples. The pooled standard deviations calculate to 9.1, 8.6, 12.5, 8.8 per meg for the Vostok, new GISP2, GISP2 (Blunier et al., 2002), and Siple Dome (Blunier et al., 2002) samples, respectively.

The underlying time scale for the study is the orbitally tuned Vostok time scale from Suwa and Bender (2008). The GISP2 and Siple Dome time scales are synchronized to Vostok via their respective  $\text{CH}_4$  records. Although there is a pole to pole  $\text{CH}_4$  gradient of up to 10 ‰, concentration changes must coincide between the two hemispheres. It turns out that the original Meese and Sowers gas time scale (Meese et al., 1994) generally agrees reasonably well with the Suwa and Bender (2008) Vostok time scale. However, for samples older than about 80 ka, a significant offset exists. We therefore adjusted the lower portion of the GISP2 gas time scale to the Vostok gas time scale at the prominent  $\text{CH}_4$  changes. The

Siple Dome samples are put on the same GISP2 gas time scale based on methane and  $\delta^{18}\text{O}$  of  $\text{O}_2$  control points (Brook et al., 2005). The  $\text{CH}_4$  data is plotted in Fig. 1 with identical colors as the  $^{17}\Delta$  data (Brook et al., 2005; Petit et al., 1999; Blunier and Brook, 2001).

Additional data necessary for the interpretation of the  $^{17}\Delta$  record were taken from the literature.  $\delta^{18}\text{O}$  of  $\text{O}_2$  data are from the Vostok ice core (Petit et al., 1999). The  $\text{CO}_2$  data are a compilation of data from Vostok, Taylor Dome and EPICA Dome C (see Lüthi et al., 2008 for original references). All data have been transferred to the Suwa and Bender (2008) time scale. For  $\delta^{18}\text{O}$  of ocean water, we rely on the ocean cores V19-30 and V19-28 following Shackleton (2000). The data is on the original Shackleton (2000) orbital time scale. In order to represent the change in  $\delta^{18}\text{O}$  of seawater, we scaled the data so that the glacial-interglacial difference is 1 ‰, with 0 ‰ for present values (Schrag et al., 2002).

$\text{CO}_2$ ,  $^{17}\Delta$  and  $\delta^{18}\text{O}$  of ocean water and  $\text{O}_2$  data were interpolated and smoothed with a Gaussian filter with  $\sigma = 1.5$  ka. Where applicable, the data were weighted relative to the precision of the individual datum.

$^{17}\Delta$  of paleoatmospheric  $\text{O}_2$  is expressed with air  $\text{O}_2$  as the standard gas. However, this standard is itself “anomalous” – the  $^{17}\Delta$  of air  $\text{O}_2$  is depleted versus ocean water. The exact magnitude of mass independent fraction in modern  $\text{O}_2$  has been a source of debate (see Barkan and Luz, 2011, for details). We initially use the Barkan and Luz (2005) value of 173 per meg for ocean water vs. the recent atmosphere for our calculations and included the presently accepted value of 223 per meg in revision.

The dominant feature of the  $^{17}\Delta$  record is its anticorrelation with the paleoatmospheric  $\text{CO}_2$  concentration (Figs. 1, A1). The sign reflects the direction of stratospheric fractionation:  $\text{O}_2$ – $\text{CO}_2$  exchange increases  $^{17}\Delta$  of  $\text{CO}_2$  and decreases  $^{17}\Delta$  of  $\text{O}_2$ . The magnitude of the  $\text{O}_2$ – $\text{CO}_2$  exchange depends on the presence of  $\text{CO}_2$  in the stratosphere. The absolute value of  $^{17}\Delta$  depends on the choice of reference, which for us is  $\text{O}_2$  in modern air. Preindustrial  $\text{CO}_2$  is unusually high for the length of our record, and  $^{17}\Delta$  of  $\text{O}_2$  is unusually low; most Vostok samples therefore have  $^{17}\Delta > 0$ , and glacial samples have the highest values.

The slope of the historical  $^{17}\Delta$  vs.  $\text{CO}_2$  plot is  $-0.36$  per meg/ppm  $\text{CO}_2$  and intercepts zero  $\text{CO}_2$  at 103 per meg (Fig. A1). In theory, one would expect that for no  $\text{CO}_2$  in the atmosphere  $^{17}\Delta$  of  $\text{O}_2$  reaches the ocean value, and that for each ppm of  $\text{CO}_2$  in the preindustrial atmosphere (280 ppm)  $^{17}\Delta$  gets depleted by 0.6 to 0.8 per meg depending on the actual value of ocean water vs. the modern atmosphere (see Barkan and Luz, 2011, for details). The difference is due to the fact that 2 factors in addition to  $\text{CO}_2$  influence  $^{17}\Delta$  on glacial–interglacial timescales. First, individual processes that fractionate  $^{17}\text{O}$  and  $^{18}\text{O}$  mass-dependently with  $\lambda$  values differing slightly from 0.516 act more or less rapidly, leading to a greater or lesser impact on the  $^{17}\Delta$  of  $\text{O}_2$  in air. As their relative influence changes, so does the mass dependent

fractionation of  $^{17}\text{O}$  with respect to  $^{18}\text{O}$ . Following our modeling approach in Sect. 4, we find that for the modern atmosphere about 60 of the 173 per meg of the anomaly can be explained by mass dependent processes. Second, gross  $\text{O}_2$  production changes. Increases attenuate the mass independent fractionation of  $\text{O}_2$  in the atmosphere, and cause the magnitude of the anomaly to decrease relative to seawater, and to increase relative to modern air. The following discussion isolates the main influences on the  $^{17}\Delta$  of past  $\text{O}_2$  in order to draw conclusions about changes in gross production through time.

#### 4 Background

The natural  $\text{O}_2$  and C cycles provide a context for understanding variations in the  $^{17}\Delta$  of  $\text{O}_2$ . The turnover time of  $\text{O}_2$  in the modern atmosphere is of order  $10^3$  a (Bender et al., 1994). Our basic understanding of the carbon cycle strongly suggests that over time less than a million years or so, atmospheric  $\text{O}_2$  should be at a steady-state in which production by photosynthesis very nearly balances consumption, and the concentration is nearly constant. This inference is now confirmed by analyses of  $\text{O}_2/\text{N}_2$  in the modern atmosphere (e.g. Manning and Keeling, 2006) and in ice cores (Bender, 2002). According to Bender et al. (1994), about 60 % of gross photosynthesis and respiration is due to the land biosphere and 40 % due to the ocean biosphere, a value also found by model simulations (Hoffmann et al., 2004). Seawater is the ultimate source of all  $\text{O}_2$  in air, since land plants derive their  $\text{O}_2$  from leaf water, which comes from precipitation and ultimately from the oceans.

Blunier et al. (2002) derived analytical equations for  $\delta^{17}\text{O}$  and  $\delta^{18}\text{O}$  of atmospheric  $\text{O}_2$  at steady-state given ocean fluxes, land fluxes, fractionation factors associated with substrate water (important for land plants) and  $\text{O}_2$  consumption, and isotope exchange in the stratosphere between  $\text{O}_2$  and  $\text{CO}_2$ . The basic approach involves setting the production rate of each isotopologue of  $\text{O}_2$  equal to its consumption rate, and solving the equations for the ratio of singly substituted isotopologues to  $^{16}\text{O}_2$  (i.e.  $^{17}\text{O}^{16}\text{O}/^{16}\text{O}_2$  and  $^{18}\text{O}^{16}\text{O}/^{16}\text{O}_2$ ). Rather than repeat the derivations, we discuss the relevant terms. The analytical equation (Eq. 15 of Blunier et al., 2002), cast in terms of  $^{18}\text{O}/^{16}\text{O}$ , is

$$R_{\text{atm}} = \frac{F_{\text{lp}}\alpha_{\text{lp}}R_{\text{sw}} + F_{\text{op}}\alpha_{\text{op}}R_{\text{sw}}}{F_{\text{lr}}\alpha_{\text{lr}} + F_{\text{ors}}\alpha_{\text{*}}\alpha_{\text{ors}} + F_{\text{ord}}\alpha_{\text{*}}\alpha_{\text{ord}} + F_{\text{str}}(1 - \alpha_{\text{str}})}. \quad (2)$$

$R_{\text{atm}}$  is the ratio of  $^{18}\text{O}/^{16}\text{O}$  in air  $\text{O}_2$ , and  $R_{\text{sw}}$  is the  $^{18}\text{O}/^{16}\text{O}$  ratio of seawater.  $F$  are fluxes of elemental oxygen in units of  $\text{mol a}^{-1}$ .  $\alpha$ s are kinetic fractionation factors for the various processes. The subscript “lp” corresponds to land photosynthesis, “sw” to seawater, “op” to ocean photosynthesis, “lr” to land respiration, “ors” to ocean surface respiration, “ord” to ocean deep respiration, and “str” to the stratosphere.

The terms in the numerator refer to global fluxes of oxygen isotopes, normalized to the seawater  $^{18}\text{O}/^{16}\text{O}$  ratio, associated with ocean productivity and land productivity. The terms in the denominator refer to normalized global fluxes of oxygen associated with respiration in surface ocean water, deep ocean water, the land biosphere, and stratospheric exchange. Oceanic  $\text{O}_2$  production is balanced by respiration in the surface and deep ocean realms. The stratosphere term is positive for the flux of  $^{18}\text{O}$  from  $\text{O}_2$  to  $\text{CO}_2$ .  $\alpha_{\text{str}}$  is a pseudo-fractionation factor that accounts for change in the  $\delta^{17}\text{O}$  and  $\delta^{18}\text{O}$  of  $\text{O}_2$  as air passes through the stratosphere. There is an analogous equation for the  $^{17}\text{O}/^{16}\text{O}$  ratio.

We follow with details of the rates and fractionation factors that we invoke to solve the equations. We make the approximation that  $^{16}\text{O}_2$  fluxes are the same as  $\text{O}_2$  fluxes; this approximation has no effect whatsoever on the outcome.

#### 4.1 Isotopic mass balance of $\text{O}_2$ in the modern (pre-industrial) atmosphere

The production rate of  $^{18}\text{O}$  ( $\text{mol} \cdot \text{a}^{-1}$ ) by terrestrial photosynthesis is given by the following equation:

$$\text{Production of } ^{18}\text{O} = F_{\text{lp}} \left( \frac{^{18}\text{O}}{^{16}\text{O}} \right)_{\text{lp}}. \quad (3)$$

To calculate  $F_{\text{lp}}$ , we adopt the estimate of Joos et al. (2004) for the rate of gross primary carbon production (carbon GPP). For the Holocene they give a value of  $1.15 \times 10^{16} \text{ mol(C)} \cdot \text{a}^{-1}$ . This number does not include carbon fixed and then burned by photorespiration. We partition production between C3 and C4 plants using the estimate of François et al. (1998) that C4 plants account for 27.5 % of GPP. We assume zero photorespiration in C4 plants and scale production of C3 plants to account for photorespiration according to the following equation derived by von Caemmerer and Farquhar (1981):

$$\frac{\text{Dark resp.} + \text{Photoresp.}}{\text{Dark resp.}} = \left( \frac{4.5}{4} \right) \left( \frac{\text{CO}_2 \cdot (p_i/p_a) + (7/3) \cdot \Gamma_*}{\text{CO}_2 \cdot (p_i/p_a) - \Gamma_*} \right). \quad (4)$$

The  $\text{CO}_2$  compensation point ( $\Gamma_*$ ) is 34 ppm.  $p_i/p_a$  is the ratio of  $\text{CO}_2$  inside the leaf to the atmospheric value; we adopt a value of 0.65.  $p_a$  is the preanthropogenic  $\text{CO}_2$  concentration, 281 ppm. We multiply by 1.07 to scale  $\text{CO}_2$  fluxes to  $\text{O}_2$  fluxes (Keeling, 1988), and divide by 0.9 assuming that the Mehler reaction accounts for 10 % of all  $\text{O}_2$  consumption (hence requiring an additional source of  $\text{O}_2$  not accounted for in the carbon flux). We thus calculate that gross photosynthetic  $\text{O}_2$  production of terrestrial ecosystems =  $2.34 \times 10^{16} \text{ mol(O}_2) \cdot \text{a}^{-1}$ .

Based on Guy et al. (1993) and Barkan and Luz (2005), there is no isotopic fractionation associated with water splitting during photosynthesis. This finding has recently been questioned. Luz and Barkan (2011) find a significant

fractionation associated with marine photosynthesis. In the course of this manuscript we adopt their value of +4‰ fractionation in  $\delta^{18}\text{O}$  versus the substrate water, and we assume a value for these processes  $\lambda$  of 0.524. Photosynthetic  $\text{O}_2$  fractionation in land plants remains to be measured; throughout this discussion we assume it is zero.

The  $^{18}\text{O}/^{16}\text{O}$  ratio of  $\text{O}_2$  produced by land photosynthesis ( $^{18}\text{O}/^{16}\text{O}$ )<sub>lp</sub> differs from the equivalent ratio in seawater for two reasons. First, rainwater or groundwater is fractionated during the hydrologic cycle by evaporation and condensation. Second, evapotranspiration leads to isotopic fractionation of water in leaves. Farquhar et al. (1993) estimated that the productivity-weighted  $\delta^{18}\text{O}$  of continental precipitation is  $-7.9\text{‰}$ . Productivity-weighted  $\delta^{17}\text{O}$  of continental precipitation is then estimated using the observed value of  $\lambda$  for meteoric waters, 0.528 (Li and Meijer, 1998). It was observed recently that the  $^{17}\Delta$  of meteoric water, calculated using the hydrologic slope of 0.5281, was further elevated by the kinetic isotope effects associated with evaporation from seawater (Landais et al., 2008). This observation, based on the isotopic composition of snow collected along a transect from the Antarctic coast to Vostok, was confirmed by a limited number of meteoric water observations mainly from Europe (Landais et al., 2006). The global productivity-weighted average of the effect, linked to humidity and wind speed, is unknown. For the Holocene we assume a value of 40 per meg. The change of this precipitation water anomaly will be relevant when we do calculations pertaining to the past.

The heavy isotopes are enriched in leaf water during the process of evapotranspiration. The enrichment is due both to kinetic processes ( $\text{H}_2^{16}\text{O}$  evaporates faster) and equilibrium processes ( $\text{H}_2^{16}\text{O}$  is enriched in the vapor phase relative to the liquid). The enrichment of  $^{18}\text{O}$  in leaf water reflects the relative importance of kinetics and equilibrium with atmospheric water vapor, which in turn depends on humidity. The ratio of  $^{18}\text{O}/^{16}\text{O}$  in leaf water normalized to that in seawater, expressed as a fractionation factor, is then given by the following equation:

$$\alpha_{lp} = (\alpha_{stem}(1-h)\alpha_k + h \cdot \alpha_v)\alpha_{eq} \quad (5)$$

$\alpha_{stem}$  expresses the GPP-weighted isotopic difference between precipitation and seawater ( $-7.8\text{‰}$ ), and  $\alpha_v$  expresses this difference between water vapor and sea water ( $-18.2\text{‰}$ ), in both cases as a fractionation factor (Farquhar et al., 1993).  $h$  is relative humidity,  $\alpha_k$  is the fractionation factor associated with evaporation, and  $\alpha_{eq}$  is the fractionation factor for water gas in equilibrium with liquid water. Fractionations associated with vapor–liquid equilibrium and with the evaporation of water into dry air are summarized in Table 2.

The magnitude of the  $^{17}\text{O}$  enrichment relative to that of  $^{18}\text{O}$  also depends on the relative importance of kinetic and equilibrium processes and is critical for our calculations. To determine  $\alpha_{lp}$  for  $^{17}\text{O}$ , we rely on the study by Landais et al. (2006), who found that the slope for evapotranspiration

( $\lambda_{Ev}$ ) is dependent on the relative humidity as  $\lambda_{Ev} = 0.522 - 0.008 \cdot h$ . We calculate  $^{17}\alpha_{lp}$  using Eq. (5), which is also valid for  $^{17}\text{O}$ , as

$$^{17}\alpha_{lp} = ^{17}\alpha_{stem} ^{17}\alpha_{EV} = ^{17}\alpha_{stem} \left( ^{18}\alpha_{EV} \right)^{\lambda_{Ev}} \quad (6)$$

or

$$^{17}\alpha_{lp} = ^{17}\alpha_{stem} \left[ \left[ (1-h) ^{18}\alpha_k + h ^{18}\alpha_v / ^{18}\alpha_{stem} \right] \cdot ^{18}\alpha_{eq} ^{18}\alpha_{EV} \right]^{\lambda_{Ev}} \quad (7)$$

GPP-weighted humidity is a tunable parameter in our calculations. We constrain average global humidity to the value that predicts a  $\delta^{18}\text{O}$  for leaf water that, together with fixed terms, correctly simulates the  $\delta^{18}\text{O}$  in  $\text{O}_2$ .

Invoking the fact that respiration closely balances photosynthesis, the consumption rate of  $^{18}\text{O}$  by terrestrial ecosystems can be expressed as

$$\text{Consumption of } ^{18}\text{O} = F_{lp} \left( ^{18}\text{O}/^{16}\text{O} \right)_{\text{atm}} \cdot ^{18}\alpha_{lr} \quad (8)$$

$^{18}\alpha_{lr}$  is the fractionation factor associated with terrestrial  $\text{O}_2$  consumption, including heterotrophic respiration in soils (including leaf litter). Evaluating this term is complex because there are at least 5 important biochemical pathways by which  $\text{O}_2$  is consumed: the light pathways of photorespiration and the Mehler reaction, the dark pathways of the mitochondrial electron transport chain, the alternative (cyanide-resistant) pathway, and chlororespiration. We neglect chlororespiration because there is no basis for estimating its significance at the present time. We apportion weights to the other pathways according to our estimates of the relative  $\text{O}_2$  fluxes associated with each, and calculate a weighted average of isotope effects based on recent measurements of fractionation factors. Our calculation assumes that the Mehler reaction accounts for 10% of  $\text{O}_2$  consumption. According to Eq. (4) photorespiration by C3 plants accounts for 38%, and mitochondrial respiration for 52% of  $\text{O}_2$  consumption. Following assumptions in Landais et al. (2007), we partition mitochondrial respiration into soil respiration (63% of dark respiration (Schlesinger and Andrews, 2000)) and leaf respiration, where 10% of the dark respiration in leaves is through the alternative oxidase pathway (Angert et al., 2003b). The isotope effect expressed in soil respiration is much less than in leaf respiration – much soil  $\text{O}_2$  consumption apparently takes place in microenvironments, where diffusion attenuates the biochemical isotope effect. Soil fractionation is also temperature-dependent (Angert et al., 2003a). For the present day (Holocene) case, we adopt the global mean value calculated by Landais et al. (2007). The weighted average isotope effect associated with terrestrial  $\text{O}_2$  consumption is then 18.00‰. The corresponding fractionation factor for  $^{17}\text{O}$  is calculated using  $\lambda$  values summarized in Table 1.

Modern ocean  $\text{O}_2$  GPP is taken from Blunier et al. (2002).  $\text{O}_2$  GPP is calculated by scaling global  $^{14}\text{C}$  production (Field

**Table 1.** Land respiration at present and during the LGM.

	$^{17}\epsilon$ (‰)	$^{18}\epsilon$ (‰)	$\lambda$	Fraction modern	Fraction LGM
Mehler reaction	-5.685	-10.800 <sup>a</sup>	0.525 <sup>a</sup>	10 %	10 %
Photorespiration	-10.950	-21.400 <sup>a</sup>	0.509 <sup>a</sup>	38 %	44 %
Dark respiration in soil <sup>d</sup>	-8.080	-15.600 <sup>b</sup>	0.516 <sup>c</sup>	33 %	29 %
Dark respiration in leaves	-9.329	-18.000 <sup>d</sup>	0.516 <sup>c</sup>	17 %	15 %
Alternative oxidase	-15.534	-30.000 <sup>e</sup>	0.514 <sup>c</sup>	2 %	2 %
Modern weighted average	-9.282	-17.998	0.5134		
LGM weighted average	-9.878	-19.161	0.5131		

Fractionation factors are given in ‰ as  $\epsilon = (\alpha - 1)$ . (a) Calculated from Helman et al. (2005). (b) The value given is for Holocene conditions (Landais et al., 2007). For the LGM we assume here 5 °C lower soil temperatures resulting in  $^{18}\epsilon$  dark soil of -18.650 (Angert et al., 2003b). (c) Angert et al. (2003b). (d) Guy et al. (1992, 1993). (e) Ribas-Carbo et al. (2000). The partitioning between the different pathways depends on the occurrence of C3 and C4 plants. Here we used 27.5 % and 40 % C4 GPP C for present and LGM, respectively (see text).

**Table 2.** Model parameters: Slope.

Var	Description	$^{17}\text{O}$	$^{18}\text{O}$
$\epsilon_*$	Equilibrium fractionation between dissolved and atmospheric $\text{O}_2$ (based on Reuer et al., 2007; Luz and Barkan, 2009; see Appendix A2)	calculated	$0.8746 - 0.0083 \cdot T$ (°C) ‰
$\epsilon_{\text{ors}}$	Mean fractionation during respiration in the marine mixed layer (Quay et al., 1993; Hendricks et al., 2004; Angert et al., 2003b)	-11.413 ‰*	-22.000 ‰
$\epsilon_{\text{ord}}$	Mean fractionation during decomposition of organic carbon in the ocean interior (Bender et al., 1994)	-6.210 ‰*	-12.000 ‰
$\epsilon_k$	Kinetic isotope fractionation between liquid and gaseous water (Farquhar et al., 1989)	not used	26.500 ‰
$\epsilon_{\text{eq}}$	Equilibrium isotope fractionation between liquid and gaseous water (Bottinga and Craig, 1969)	not used	9.150 ‰
$\epsilon_{\text{stem}}$	GPP-weighted precipitation water versus SMOW (Farquhar et al., 1993; Li and Meijer, 1998)	-4.172 ‰*	-7.900 ‰
$\epsilon_V$	GPP-weighted precipitation water vapor versus SMOW (Farquhar et al., 1993; Li and Meijer, 1998)	-9.611 ‰*	-18.200 ‰
$\epsilon_{\text{str}}$	Fractionation in the stratosphere	$-1.065 \times 10^{-3}$ ‰ <sup>+</sup>	$-0.625 \times 10^{-3}$ ‰ <sup>+</sup>
$\epsilon_{\text{lp}}$	Leaf water enrichment (summed fractionations from ocean to leaves)	3.458 ‰ <sup>+</sup>	6.791 ‰ <sup>+</sup>

\* Calculated from  $^{18}\text{O}$  and  $\lambda$  or  $\gamma$ , + calculated during the initialization.

et al., 1998) for the ratio of  $\text{O}_2$  GPP/ $^{14}\text{C}$  production measured in vitro (Bender et al., 2000). The calculated value is then  $1.09 \times 10^{16}$  mol ( $\text{O}_2$ )  $\text{a}^{-1}$ . The  $\delta^{18}\text{O}$  and  $\delta^{17}\text{O}$  of photosynthetic  $\text{O}_2$  are identical to seawater (zero on the SMOW scale). 95 % of the organic matter is consumed in surface water and 5 % in deep water (Bender et al., 1994). The  $^{18}\text{O}$  respiratory isotope effect is 22 ‰ for remineralization in surface water (Quay et al., 1993; Hendricks et al., 2004) and 12 ‰ in deep water (Bender et al., 1994). The surface value likely includes intracellular recycling of new photosynthetic  $\text{O}_2$  with a consequent  $\delta^{18}\text{O}$  enrichment as recognized by Eisenstadt et al. (2010). The surface water number is empirically constrained by the  $^{18}\text{O}$  balance of the mixed layer. The subsurface value does not reflect a difference in fractionation at

the cellular level. Rather, it signifies that the  $^{18}\text{O}$  increase associated with respiration is not fully expressed because it is attenuated by mixing (Bender et al., 1994).  $\lambda$  for the dark ocean is calculated assuming that 10 % of  $\text{O}_2$  consumption is by the alternative oxidase ( $\alpha = 0.970$  (Ribas-Carbo et al., 2000), and  $\lambda = 0.514$  (Angert et al., 2003b)) and 90 % is by mitochondrial respiration ( $\alpha = 0.982$  and  $\lambda = 0.516$  (Helman et al., 2005), corresponding to a  $\gamma$  value of 0.518). The weighted  $\lambda$  value for the dark ocean is then 0.516. For the surface ocean we assume 5 % photorespiration ( $\lambda = 0.509$ ) and 10 % Mehler reaction ( $\lambda = 0.496$ ) (Helman et al., 2005). The remaining 85 % is distributed between alternative oxidase and mitochondrial respiration in the ratio 1 : 9, resulting in  $\lambda = 0.514$ .

In our approach we treat the stratospheric exchange as a fractionating process applied to air passing through the stratospheric box, characterized by values of  $^{17}\alpha$  and  $^{18}\alpha$ . In Eq. (2)  $F_{\text{strat}}$  is the flux of oxygen through the stratosphere, and  $\alpha_{\text{strat}}$  is the virtual isotopic fractionation realized if we assume that  $\text{O}_2$  in air exiting the stratosphere is uniformly depleted in  $^{17}\text{O}$  or  $^{18}\text{O}$ . It has been observed that  $\delta^{17}\text{O}$  of stratospheric  $\text{CO}_2$  covaries with  $\delta^{18}\text{O}$ , with a slope of 1.7 (Boering et al., 2004; Lämmerzahl et al., 2002). The exchange will cause  $\text{O}_2$  isotopes to vary with a similar slope.

Dissolved  $\text{O}_2$  at equilibrium with air is fractionated versus the free atmosphere. Reevaluating two studies (Reuer et al., 2007; Luz and Barkan, 2009; see Appendix A2) we find

$$\varepsilon_* = 0.8746 - 0.0083 \cdot T(\text{‰}) \text{ and } \lambda = 0.5284 \pm 0.0017, \quad (9)$$

where  $T$  is the ocean temperature in  $^{\circ}\text{C}$ .

Values for the isotopic properties on the modern Earth are summarized in Table 2, and values for the flux properties on the modern Earth are summarized in Table 3. The discussion above leaves unspecified two variable properties in the two equations for the pre-industrial isotope ratios for  $^{17}\text{O}$  and  $^{18}\text{O}$  (Eq. 4). One (referred to earlier) is the GPP-weighted humidity ( $h$ ). The second is the stratospheric fractionation ( $^{18}\alpha_{\text{strat}}$ ). We constrain these parameters to values simulating  $\delta^{18}\text{O}$  and  $\delta^{17}\text{O}$  for leaf water that, given other values adopted here, correctly predict  $\delta^{18}\text{O}$  and  $\delta^{17}\text{O}$  of  $\text{O}_2$  observed for the modern atmosphere (Tables 2 and 3).

The calculated value for GPP-weighted humidity depends on two factors. The first is the adopted  $^{17}\Delta$  value of the modern atmosphere vs. ocean water. The second is the presence and magnitude of the ocean photosynthetic fractionation. The calculated range of relative humidity, between 57 % and 62 %, pertains to the daytime atmosphere. These values are significantly lower than the true global average of about 67 %. However, during the day, and over the biologically active portion of the year, relative humidity is generally significantly lower than the yearly average. Especially in the tropics, relative daytime humidity is of the order of 55 % as seen in a present-day simulation with the NCAR CCM3 atmospheric general circulation model (Kiehl et al., 1998; Peter Langen, personal communication, 2009). We conclude that our value for GPP-weighted humidity is of the right magnitude. The accompanying values of the global leaf water  $\delta^{18}\text{O}$ , +6.8 ‰ to +5.0 ‰, lie within the range of previous studies (see Hoffmann et al., 2004, for a compilation of previous findings).

From our model initialization we calculate net  $^{17}\text{O}^{16}\text{O}$  and  $^{18}\text{O}^{16}\text{O}$  fluxes across the tropopause of  $3.9 \times 10^9$  and  $1.3 \times 10^{10}$  mol, respectively. These are the fluxes constrained by Eq. (2) as applied to  $^{17}\text{O}^{16}\text{O}$  and  $^{18}\text{O}^{16}\text{O}$ , and the parameters whose values we have specified. We compare these numbers with an independent estimate that we derive as follows from stratospheric data. We use data on the  $\Delta^{17}\text{O}$  of  $\text{CO}_2$  in the stratosphere, the linear scaling of  $\Delta^{17}\text{O}$  and  $\text{N}_2\text{O}$

concentration (which decreases because of loss by photolysis), and an estimate of the rate of the  $\text{N}_2\text{O}$  photolysis to calculate the stratospheric transfer rate of  $^{17}\text{O}$  and  $^{18}\text{O}$  from  $\text{CO}_2$  to  $\text{O}_2$  (Boering et al., 2004). We can then calculate the net flux of anomalous  $\text{O}_2$  into the troposphere. Following Boering et al. (2004), we restrict analyses of  $\Delta^{17}\text{O}$  vs.  $\text{N}_2\text{O}$  to regions where  $\text{N}_2\text{O}$  concentrations are below 195 ppb (parts per billion by volume), and calculate slopes of  $\text{C}^{18}\text{O}^{16}\text{O}:\text{N}_2\text{O}$  concentrations. Multiplying this number with the net loss rate of  $\text{N}_2\text{O}$ ,  $12.5 \text{ Tg a}^{-1}$  (Denman et al., 2007), gives the net production rate of  $\text{C}^{18}\text{O}^{16}\text{O}$  (see, for example, Plumb and Ko, 1992). The fractional loss of  $^{17}\text{O}^{16}\text{O}$  is 1.7 times the fractional loss of  $^{18}\text{O}^{16}\text{O}$ . The net  $\text{CO}_2$  flux matches the net  $\text{O}_2$  flux. We calculate the net  $\text{O}_2$  flux across the tropopause as  $3.1 \pm 0.9 \times 10^9$  and  $1.1 \pm 0.4 \times 10^{10}$  mol  $^{17}\text{O}^{16}\text{O}$  and  $^{18}\text{O}^{16}\text{O}$ , respectively. These fluxes are in good agreement to the fluxes calculated from our model initialization when scaled for the lower pre-anthropogenic  $\text{CO}_2$  concentration and given the uncertainties with initialization parameters (e.g. fractionation factors and fluxes) and flux calculations (e.g. 25 % for  $\text{N}_2\text{O}$  flux, Ehhalt et al., 2001).

#### 4.2 Isotopic mass balance of $\text{O}_2$ in the glacial atmosphere

During glacial times fluxes are of course different from the present. In addition, several parameters differ from their interglacial values. Process-level fractionation factors (e.g. for photosynthesis, Mehler reaction, etc.) remain at their interglacial values except for stratospheric pseudo fractionation. For the stratospheric effect we assume that the net fluxes of  $^{17}\text{O}^{16}\text{O}$  and  $^{18}\text{O}^{16}\text{O}$  into the troposphere scale linearly with the  $\text{CO}_2$  concentration of air. This assumption aligns with the chemical kinetic model of Yung et al. (1997) for stratospheric  $\text{O}_2\text{--CO}_2$  exchange.

The effective fractionation factor for terrestrial  $\text{O}_2$  consumption changes due to the different partitioning of C3 and C4 plants, and because photorespiration by C3 plants is a function of the  $\text{CO}_2$  concentration. A further influence comes from the temperature dependence of the fractionation associated with soil respiration.

The isotope signature of oxygen produced by land photosynthesis depends on the signature of the precipitation water. Model simulations for the Last Glacial Maximum from Atmospheric Global Circulation Models (AGCM) show a 0–1 ‰ increase in the  $\delta^{18}\text{O}$  of precipitation compared to the interglacial (Jouzel et al., 2000). This change translates into a nearly constant fractionation for the hydrological cycle between glacial and interglacial. There is, however, a tendency for a shift to lower isotope values in ice free areas above about  $45^{\circ}\text{N}$  of about  $-2$  to  $-4$  ‰. Continental productivities in such regions were very low during the LGM.

A parameter that affects the  $^{17}\text{O}$  anomaly of  $\text{O}_2$  produced by the land biosphere is the anomaly in the precipitation



**Table 3.** Isotope ratios and fluxes.

Var	Description	$^{17}\text{O}$	$^{18}\text{O}$
$R_{\text{sw}}$	Abundance relative to $^{16}\text{O}$ , SMOW (Hoefs, 1996)	$3.73000 \times 10^{-4}$	$2.00520 \times 10^{-3}$
	Fractionation of air $\text{O}_2$ versus SMOW (Barkan and Luz, 2005)	12.08 ‰	23.88 ‰
$R_{\text{atm}}$	Abundance relative to $^{16}\text{O}$ in $\text{O}_2$ (calculated from values above)	$3.77506 \times 10^{-4}$	$2.05308 \times 10^{-3}$
$F_{\text{op}}$	Gross photosynthetic oxygen flux from the ocean biosphere (see text for details)	$1.09 \times 10^{16} \text{ mol O}_2 \text{ a}^{-1}$	
$F_{\text{ors}}$	Mixed layer respiration	$0.95 \times F_{\text{op}}$	
$F_{\text{ord}}$	Deep ocean respiration	$0.05 \times F_{\text{op}}$	
$F_{\text{lp}}$	Gross photosynthetic oxygen flux from the land biosphere (see text for details)	$2.34 \times 10^{16} \text{ mol O}_2 \text{ a}^{-1}$	
$F_{\text{str}}$	Stratosphere–troposphere oxygen exchange flux (Appenzeller et al., 1996)	$4.9 \times 10^{18} \text{ mol O}_2 \text{ a}^{-1}$	

**Table 4.** Values for the LGM sensitivity study.

$^{17}\Delta$ of $\text{O}_2$ (per meg)	$\text{CO}_2$ (ppmv)	$\delta^{18}\text{O}_{\text{atm}}$ (‰)	$\delta^{18}\text{O}$ ocean (‰)
40	189	1	1

water. In central Antarctica (Vostok) the anomaly in precipitation water dropped from about 40 per meg to roughly 15 per meg in the glacial (Landais et al., 2008). This change suggests a wetter atmosphere (higher humidity) above the source region for Antarctic precipitation during the glacial (Landais et al., 2008). Other stations in Antarctica show little or no change in the precipitation anomaly (Winkler et al., 2012). Finally, the isotopic composition of leaf water depends on relative humidity, because isotope fractionation during evapotranspiration depends on the balance of equilibrium and kinetic processes. Therefore, humidity also has a large influence on the isotopic composition of  $\text{O}_2$  produced by the land biosphere.

In a sensitivity study we now examine the influence of some parameters in the context of a scenario for the Last Glacial Maximum (LGM). The input values for this scenario are calculated as the mean values for the time period 25–18 ka before present (BP) (Table 4). Based on Eq. (2) we calculate gross land and ocean  $\text{O}_2$  production. The basic constraints in the following calculations are the glacial atmospheric  $\delta^{18}\text{O}$  and  $^{17}\Delta$  signatures. The results are summarized in a 3-D plot of LGM properties (land biosphere production as a function of modern, ocean biosphere production as a function of modern, and glacial–interglacial change in soil temperature).

In these calculations, we adopt a value of +173 per meg for the  $^{17}\Delta$  of ocean water, with modern atmospheric  $\text{O}_2$  as the reference. We also assume that there is no fractionation between  $\text{O}_2$  and water during marine photosynthesis. Our default scenario (blue grid in Fig. 2) invokes the initialization values of the (GPP-weighted) anomaly of the precipitation water (39 per meg) and relative humidity (57 %). For glacial soil temperatures, we adopt values 4–7 °C (Jansen et

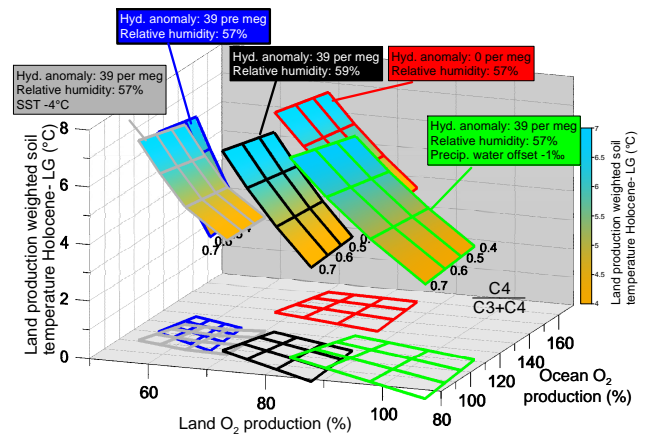


**Fig. 2.** Fluxes of land and ocean production relative to modern (100 %) for a range of C4 contributions (40–70 %) and land production-weighted soil temperatures 4–7 °C lower than modern. Blue (default scenario): relative humidity and  $^{17}\Delta$  anomaly of precipitation similar to modern (57 % humidity and 39 per meg hydrological anomaly). Relative to the default scenario the following parameters were modified: SST 4 °C lower than modern (gray-lined flying carpet), relative humidity increased from 57 % to 59 % (black-lined), hydrological anomaly set to 0 (red-lined), and precipitation  $\delta^{18}\text{O}$  1 ‰ lighter relative to paleo ocean water (green-lined). Also shown are projections of the flying carpets onto the plane, at bottom, where there was no difference between Holocene and Last Glacial Maximum temperatures. Note: all calculations for this graph are strictly for a LGM situation (Table 4). It is not possible to extract results for a Holocene situation from this graph.

al., 2007) colder than present. We then solve for land and ocean GPP, while allowing the fraction of terrestrial GPP from C4 plants to vary between 40–70 % (see Appendix A3). We then calculate land and ocean productivities of 54–66 % and 97–127 % of present, respectively. Soil temperature affects the respiratory fractionation but has a negligible effect on lambda soil. The consequence is that mainly the land production is affected by the soil temperature.

Sea surface temperature has an effect on the equilibrium fractionation of dissolved oxygen. However, the lambda value for this process is similar to the fractionation factor in



the hydrological cycle. Therefore, the lowered SST during the LGM has a small effect on the outcome of the simulations. If we lower SST by 4 °C (gray grid in Fig. 2), we obtain productivities of 53–70 % and 95–120 % of present for land and ocean, respectively, very close to the outcome of the default scenario.

Global GPP-weighted relative humidity is the most important parameter for calculating the isotope effect on oxygen produced by land plants. This is because humidity has such a strong influence on the isotopic composition of leaf water. Unfortunately, GPP-weighted humidity during the LGM is a big unknown. For a 2 % increase in relative humidity, calculated land productivity increases by 30 % relative to the default LGM scenario, while ocean productivity decreases slightly by 13 % (black grid in Fig. 2).

So far we have assumed that the global hydrological anomaly remains unchanged between today and the LGM. The available results do not tell us if this was indeed the case. At Vostok values as low as 15 per meg were found for the LGM. We calculate an extreme scenario with a hydrologic anomaly of 0 per meg. This is appropriate because the hydrologic anomaly never reaches negative values given a realistic range of humidity values (Barkan and Luz, 2007). The effect is a roughly 30 % increase in both land and ocean productivities relative to the default scenario (red grid in Fig. 2).

Another unknown is the isotopic composition of GPP-weighted precipitation water. For a 1 ‰  $\delta^{18}\text{O}$  decrease of the difference between precipitation water and ocean water (where the same difference is applied to water vapor), land production increases by 56 % relative to the default scenario, while ocean productivity decreases by 15 % (green grid in Fig. 2). All changes discussed above result in calculated changes that are larger for land than for ocean productivities, with C4 fractions between 0.4 and 0.7 and glacial temperatures between 4 and 7 °C lower than present.

Implementing the calculation with a  $^{17}\Delta$  of modern ocean water vs. modern atmosphere of 223 per meg changes the solution in the range of 20 % without changing the basic dependencies from parameters discussed above. However, allowing for O-isotope fractionation during marine photosynthesis has a quite dramatic effect on the calculations. This is mainly due to the influence on the  $\delta^{18}\text{O}$  constraint. The  $\lambda$  for the marine photosynthesis is of minor importance. The effects are exemplified in Fig. A4 for a 2 % increase in relative humidity relative to the respective initializations.

#### 4.2.1 Approach to derive ocean production in the glacial atmosphere

From the large range of land productivities that we calculate, we conclude that there are at present too many unknowns to derive both land and ocean fluxes from  $^{17}\Delta$  and  $\delta^{18}\text{O}$  of  $\text{O}_2$ . In the following discussion, we use a different approach to interpreting the 400 ka Vostok climate record. We recognize that land productivity is constrained by extensive pollen data

during the LGM and by modeling studies, whereas ocean primary productivity is less well constrained. We thus use independent estimates for land productivity in combination with  $^{17}\Delta$  to estimate ocean GPP. As before, we first focus on our scenario for the Last Glacial Maximum (Table 4). For the land productivity we adopt the values simulated by Joos et al. (2004) for C GPP by the land biosphere. The amount of  $\text{O}_2$  produced for a given GPP C is calculated as a function of the atmospheric  $\text{CO}_2$  concentration and the fraction of C4 plants (see Sect. 4.1).

We begin with Fig. 3a, which illustrates the concept of deriving both land and ocean production from  $^{17}\Delta$  and  $\delta^{18}\text{O}$  of  $\text{O}_2$  relative to today (this is the approach used in deriving Fig. 2). Calculations in Fig. 3 are based on our default LGM scenario where we assume that the  $^{17}\Delta$  of modern ocean water is 173 per meg with respect to the modern atmosphere, and do not allow for marine photosynthetic fractionation. The hydrological anomaly remains unchanged from the initialization; 39 % of terrestrial GPP is C4, and soil temperatures are 5 °C lower than modern. The heavy dashed line shows solutions that satisfy the  $\delta^{18}\text{O}$  value observed for the glacial atmosphere. The heavy solid line satisfies the  $^{17}\Delta$  values but not necessarily the  $\delta^{18}\text{O}$  or  $\delta^{17}\text{O}$  values. The intercept of the two lines gives consistent values satisfying both  $\delta^{18}\text{O}$  and  $^{17}\Delta$  constraints for land and ocean production. However, the land solution in particular is unreliable because, as noted above, it is very sensitive to the exact values of the constraining parameters. In general, land GPP values derived in this way disagree with the independent estimate for land productivity derived from Joos et al. (2004) (green line in Fig. 3b). We can tune the model solution (crossing point) by varying GPP-weighted humidity, which mainly affects the  $\delta^{18}\text{O}$  line. Increased humidity leads to a smaller heavy isotope enrichment in oxygen produced by the terrestrial biosphere, causing the calculated terrestrial productivity to rise. We estimate GPP of the ocean biosphere by adjusting average global humidity so that land GPP equals the target value (Joos et al., 2004). The blue dashed line in Fig. 3b illustrates how the  $\delta^{18}\text{O}$ – $^{17}\Delta$  intercept moves from the start point with humidity 0.572 towards the target land productivity value as we increase relative humidity. Here it is important to note that the target value (green line) for the land oxygen production depends on the C4 fraction. For a given value of land carbon GPP, a greater C4 contribution results in less oxygen cycling by photorespiration, and therefore lower  $\text{O}_2$  GPP. For our default LGM scenario, the range of 40–70 % C4 production corresponds to 63–83 % land production relative to present. We have seen in our sensitivity study (Fig. 2) that the isotopic composition of the precipitation water has a large effect on the solutions for land and ocean productivities. In the approach taken here, humidity is chosen so that land production matches the independent estimate, and the isotopic composition of precipitation is held constant. We note that humidity, our free parameter, adapts so that changes in the

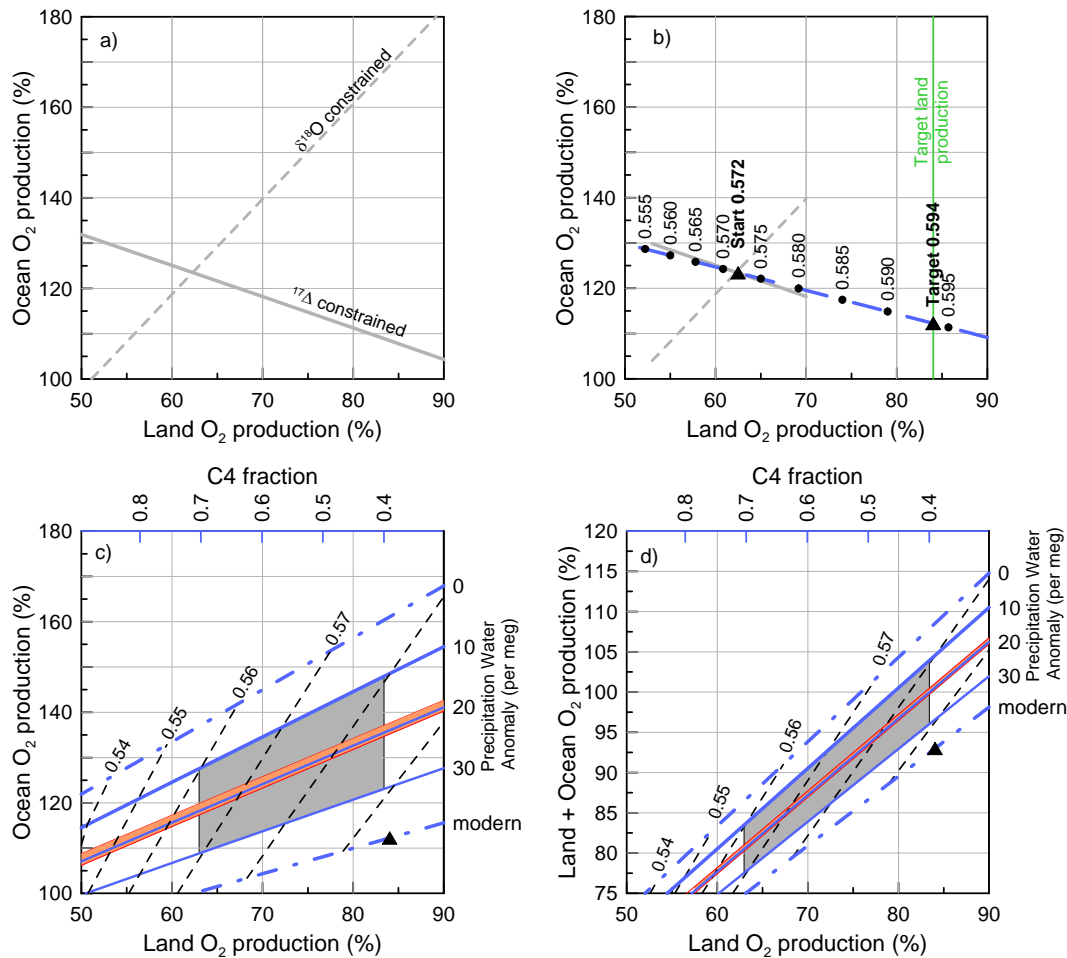


**Fig. 3.** Plots of ocean O<sub>2</sub> production vs. land O<sub>2</sub> production (a–c) and total O<sub>2</sub> production vs. land O<sub>2</sub> production (d) for the Last Glacial Maximum default scenario (see Table 4). The lines and areas indicate allowable values as constrained by the  $\delta^{18}\text{O}$  and  $^{17}\Delta$  of paleoatmospheric O<sub>2</sub> relative to the modern (100%) production. (a) Gray dashed and solid line: solutions that satisfy  $\delta^{18}\text{O}_{\text{atm}}$  and  $^{17}\Delta$ , respectively, assuming modern humidity and a hydrological anomaly similar to modern. (b) Solutions of (a) in gray. Increasing the relative humidity (black dots and associated labels) drives the intercept of  $^{17}\Delta$  and  $\delta^{18}\text{O}$  towards the target value for land productivity (see text for details). (c) and (d) The value for land carbon productivity is locked. Therefore, the land O<sub>2</sub> production is inversely proportional to the C4 contribution (top axis). We show solutions for precipitation anomalies from 0 to 40 per meg and soil temperature 5 °C lower than modern. The area in red represents solutions with soil temperatures 4–7 °C lower than modern and a precipitation  $^{17}\Delta$  anomaly of 20 per meg lower than modern. Black dashed lines show isolines of global GPP-weighted humidity. The gray area represents solutions we favor. Black triangles show the target value of (b).

fractionation of precipitation water in terms of  $\delta^{18}\text{O}$  have a negligible effect on the calculated ocean GPP.

Figure 3c, d shows solutions for our LGM scenarios for various  $^{17}\Delta$  values of the precipitation anomaly, LGM soil temperatures, and C4 fractions. The solution from Fig. 3b is shown as a black triangle sitting on the blue dashed light line representing solutions with the modern  $^{17}\Delta$  anomaly in precipitation water. The hydrological anomaly has a large effect on the solutions. A conservative estimate would be that the hydrologic anomaly could be anything between 0 and today's value of +40 per meg (heavy dash-dotted blue lines). New data from Antarctica show heterogeneous results with glacial values ranging from no change to 25 per meg lower

than modern for Vostok (Landais et al., 2006; Winkler et al., 2012). Central Antarctica shows much larger changes than the Antarctic coast. From the available data we argue that the global  $^{17}\Delta$  of precipitation was probably between 10 and 30 per meg lower than today (in the area bounded by the heavy solid blue lines).

Soil temperature affects only a small portion of the land respiration and therefore has a relatively small effect on calculated ocean productivity. This is illustrated in Fig. 3c, d for a range of 4–7 °C lower temperature than present and a hydrologic anomaly of 20 per meg lower than modern (red band). For a range of C4 contribution to land GPP of 40–70%, and a hydrological anomaly 10–30 per meg lower than

today (gray area), we calculate ocean productivities of 109–148 % of today, resulting in a total productivity of 83–104 %.

The approach can also be used applying a modern ocean water to atmosphere  $^{17}\Delta$  of 223 per meg and allowing for photosynthetic fractionation (see Appendix Fig. A5). Compared to the results presented in Fig. 3, we find that the ocean productivity barely depends on the C4 contribution. For a hydrological anomaly 10–30 per meg lower than today (gray area), we calculate ocean productivities of 95–115 % of today, resulting in a total productivity of 74–92 % of modern. Our approach basically eliminates the  $\delta^{18}\text{O}$  constraint and in that way adapts so that changes in the  $\delta^{18}\text{O}$  of precipitation water, for example, have a negligible effect on the calculated ocean GPP. This also means that  $h$  adapts to the proposed marine photosynthetic fractionation. Thus, the resulting value for  $h$  may vary while the calculated value for ocean GPP is nearly constant.

## 5 400 ka time series

We now calculate ocean (and total) productivities for the 400 ka Vostok  $^{17}\Delta$  record. Target values of land productivities as a function of atmospheric  $\text{CO}_2$  concentration are derived from the assumption that land productivity always scaled with  $\text{CO}_2$  as simulated for the past 25 ka (Joos et al., 2004). We then derive the following equation ( $R^2=0.997$ ) for land biosphere GPP as a function of atmospheric  $\text{CO}_2$  concentration:

$$\text{Land biosphere GPP (mol C yr}^{-1}\text{)} = -1.49 \times 10^{11} \times c^2 + 1.03 \times 10^{14} \times c - 5.66 \times 10^{15}, \quad (10)$$

where  $c$  is the atmospheric  $\text{CO}_2$  concentration in ppmv. This equation parameterizes terrestrial productivity in terms of  $\text{CO}_2$ , but correlative properties (temperature, ice cover, etc.) are likely to be ultimate controls. We use Eq. (10) to derive GPP C for the land productivity for the Vostok record from its  $\text{CO}_2$  context. In these calculations, we allow the fractional C4 abundance to vary between 40–70 % at full glacial conditions. For intermediate conditions, we scale C4 production according to the  $\text{CO}_2$  concentration. We also scale past hydrological anomalies, weighted for GPP, according to Vostok  $\delta\text{D}$  changes. This approach is validated by the good correlation between the hydrological anomaly and  $\delta\text{D}$  in the Vostok record (Landais et al., 2008).

Figure 4 shows solutions for 40 % and 70 % C4 contribution and for values of the hydrological anomaly during the LGM of 0–30 per meg less than the modern value. As explained above, land productivity is calculated from the  $\text{CO}_2$  concentration based on the model of Joos et al. (2004). As before, when the abundance of C4 rises, the rate of photorespiration falls, as does land GPP. Given the uncertainties in the  $^{17}\Delta$  data and parameters essential for our calculations, we do not analyze individual oscillations in our output data. The general picture (when implementing our calcula-

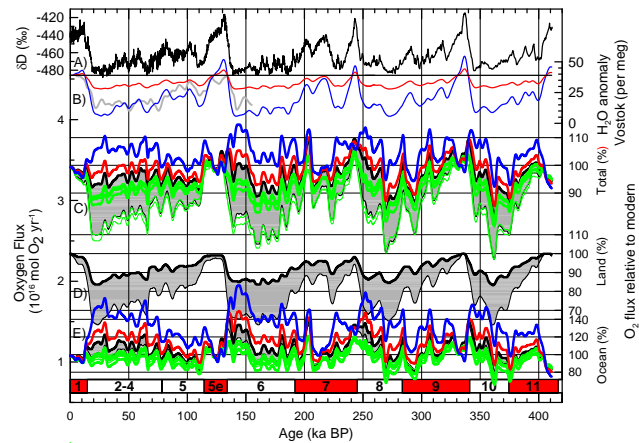


**Fig. 4.** (A)  $\delta\text{D}$  record from Vostok (Petit et al., 1999). (B) Gray solid line is the smoothed record of the  $^{17}\Delta$  anomaly in Vostok ice (Landais et al., 2008). Black, red, and blue solid lines are calculated anomalies for glacial values lower by zero, 10, and 30 per meg (see text for details). (C), (D), and (E) Total (plot C), land (D), and ocean (E) productivities relative to modern, calculated for various conditions. The black lines for land productivity are calculated from the  $\text{CO}_2$  concentration derived after the empirical findings in Joos et al. (2004) for a C4 contribution of 40 % (heavy black line) and 70 % (light black line), respectively. Heavy black, red, and blue lines for ocean and total productivities are calculated for 40 % C4 partition and relative to modern unchanged and 10 and 30 per meg lower glacial anomalies, respectively. Black light lines are calculated in the same way for unchanged glacial anomalies and 70 % C4 partitions. For better readability the solutions for 10 and 30 per meg lower glacial anomalies and 70 % C4 partitions are not shown. They lie proportionally lower relative to their respective 40 % C4 solutions, similar to the solutions for the unchanged case. All calculations except for the ones in green were made with a modern ocean water to atmosphere implementation of 173 per meg. The green lines show similar calculations but with a present ocean water vs. atmosphere value of 223 per meg. The spread of the green lines cover precipitation water anomalies 0 to 10 per meg lower than today, with and without photosynthetic fractionation of the ocean and C4 partitions of 40–70 %.

tions with a modern ocean water to atmosphere  $^{17}\Delta$  of 173 per meg) is that the oceanic oxygen productivity was elevated during glacial maxima and glacial–interglacial transitions. At the end of interglacials and beginning of glacials, ocean productivity was around modern values.

In the case where the (GPP-weighted) hydrological anomaly in the past was the same as today, the C4 partition is of minor importance for the resulting ocean productivity. With increased difference of the anomaly from today, the C4 partition becomes more important. For hydrological anomalies similar to those observed at Vostok, past values of ocean production are calculated to be 120–150 % of modern.

For the scenario in which there is no change in the  $^{17}\Delta$  anomaly of precipitation, total productivity is calculated to be slightly lower than today for glacial conditions as a result

of the lower land productivity (Fig. 4). This reduction becomes significantly greater for higher levels of C4 partition. For the 40 % C4 partition and higher  $^{17}\Delta$  anomalies in precipitation, the increase in ocean production outweighs the reduced land production.

In Blunier et al. (2002) we argued for a reduced total productivity during the glacial vs. the Holocene. This conclusion was based on the assumption of a largely reduced land productivity of 50 %. In contrast, LGM land productivity as estimated by Joos et al. (2004), adopted here, is only moderately reduced relative to the Holocene. This, together with updated values of fractionation factors, results in no change in total productivity for a scenario similar to the one used in the 2002 publication, (i.e. roughly 40 % C4 contribution and no hydrologic anomaly). Invoking an increased C4 contribution reduces the land productivity and therefore also total productivity.

Only for a constant  $^{17}\Delta$  anomaly of precipitation, and a very large glacial C4 contribution of 70 %, do we find no change in ocean productivity. We see such a scenario as unlikely (see Appendix A3). Our favored scenario includes a moderate change in the precipitation  $^{17}\Delta$  anomaly relative to today, and a moderate increase of in the glacial C4 contribution (to 40 %). According to this scenario, there is a slight increase in total productivity and an about 20 % increase in ocean productivity.

Implementing the calculations with a modern ocean water to atmosphere  $^{17}\Delta$  of 223 per meg has a large effect. As outlined before the sensitivity to the C4 contribution is much reduced, and the implementation of marine photosynthetic fractionation has a negligible effect in the approach taken here. Before, implementing the calculations with a modern ocean water to atmosphere  $^{17}\Delta$  of 173 per meg, we generally obtained results with an increased ocean productivity during glacial times. This is no longer the case; the ocean productivity was mostly around modern values, oscillating between 80–120 % at most. There are currently too many unknowns and uncertainties to judge if these oscillations might be a real feature. The total productivity is obviously very dependent on the land productivity. The reduction in land productivity compensates any increase from ocean productivity, and therefore total O<sub>2</sub> production during glacials is always smaller than during interglacials.

In a biogeochemical context, the interesting result is that ocean productivity was similar to today's value, despite major environmental differences. Perhaps the basic reason for the modest variability of GPP is that when waters are more productive and contain more chlorophyll, light is absorbed higher in the water column, and less of the ocean is illuminated. Thus, depth-integrated productivity in the euphotic zone ( $\text{mmol m}^{-2} \text{ day}^{-1}$ ) is much less variable than volumetric productivity ( $\text{mmol m}^{-3} \text{ day}^{-1}$ ) near the sea surface. Beyond doubt, ocean productivity is limited by iron, nitrogen, and/or phosphorus in most regions. However, gross production may still be high because smaller microbes, which

assimilate nutrients more easily, can dominate oligotrophic ecosystems. In addition, organisms in nutrient-poor surface waters can acquire nutrients by vertical migration (Johnson et al., 2010). There are large variations in the seawater chlorophyll concentration and primary production (generally estimated using the  $^{14}\text{C}$  method, Steemann Nielsen, 1951) (e.g. Behrenfeld and Falkowski, 1997), but recent observations challenge the idea that productivity is very low in even the most highly oligotrophic oceans (Claustre et al., 2008). Productivity may be very high during periods of blooms, but the exhaustion of nutrients terminates these periods. The same factors that temper spatial variability of gross photosynthesis in the modern ocean will also temper temporal variability in the global ocean.

One can envision many environmental changes that would cause LGM productivities to differ from modern. Factors that would suppress production include colder temperatures (and decreased metabolic rates), emergence (above sea level) of productive nearshore regions that are submerged during interglacial times, and deeper mixed layers due to stronger winds over the midlatitude oceans (e.g. Li et al., 2010). On the other hand, productivities would be enhanced by more arid conditions and greater dust transport (and iron availability to phytoplankton) (Li et al., 2010), and stronger midlatitude winds that would more rapidly recycle nutrients to the euphotic zone.

It is interesting to compare our estimates of LGM gross photosynthetic O<sub>2</sub> production with 2 estimates of net community production, which approximates carbon export from the euphotic zone. Kohfeld et al. (2005) mapped the difference, from a wide range of studies, between LGM and the Late Holocene in carbon export. They found large regional differences but an overall pattern showing no clear global trend. Bopp et al. (2003) estimated that carbon export during the LGM was about 5 % less than today. Again, the changes are very small.

## 6 Conclusions

The outcome of our calculations, and the importance of relevant parameters, depends heavily on the assumed modern ocean to atmosphere  $^{17}\Delta$  difference. While of minor importance for a difference of 223 per meg (Barkan and Luz, 2011), the extent of the C4 contribution to land production and the  $^{17}\Delta$  anomaly in precipitation water are very important when implementing the model with modern ocean to atmosphere  $^{17}\Delta$  difference of 173 per meg (Luz and Barkan, 2005).

For our default LGM scenario, we examined scenarios with a range of C4 contributions to land GPP of 40–70 % and a hydrological anomaly 10–30 per meg lower than today. In this case, we calculate ocean productivity of  $129 \pm 20\%$  and  $104 \pm 8\%$  relative to modern for an implementation of modern ocean water to atmosphere  $^{17}\Delta$  of 173 and 223 per meg,

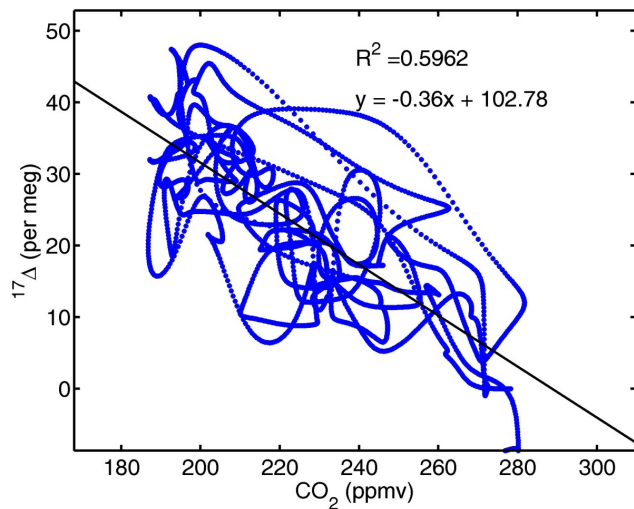


**Fig. A1**  $^{17}\Delta$  vs.  $\text{CO}_2$  from Fig. 1. See main text for details on the  $^{17}\Delta$  data. Compiled  $\text{CO}_2$  data are from Vostok, Taylor Dome and EPICA Dome C (see main text for details and references).  $\text{CO}_2$  and  $^{17}\Delta$  data are interpolated to 100 yr intervals.

respectively. The increased ocean productivity does not compensate for the reduced land productivity. Total productivity is estimated to be  $94 \pm 11\%$  and  $83 \pm 9\%$  of modern.

For the oxygen productivities calculated from our 400 ka Vostok  $^{17}\Delta$  record, we find that oceanic oxygen productivity was generally elevated by up to 20% relative to modern during glacial maxima and glacial–interglacial transitions. At the end of interglacials and beginning of glacials, ocean productivity was around modern values. For reduced hydrological anomalies relative to modern, ocean productivities rise relative to modern values except for short intervals with a climate very similar to modern. For hydrological anomalies similar to those observed at Vostok, the changes reach 150% to 120%.

However, applying the recent average value for modern ocean water to atmosphere  $^{17}\Delta$  of 223 per meg, a different picture emerges. The results with this implementation are more robust with reduced sensitivities concerning C4 partition and hydrological anomalies. Ocean productivities are mostly around modern values with no systematic link to the background climate.

We note that the calculated productivities show changes derived from  $^{17}\Delta$  variations uncoupled to any of the records, input such as that for  $\text{CO}_2$ , used for calculating productivities. This shows that there is additional information in the oxygen data unrelated to main global climate parameters like the atmospheric  $\text{CO}_2$  concentration.

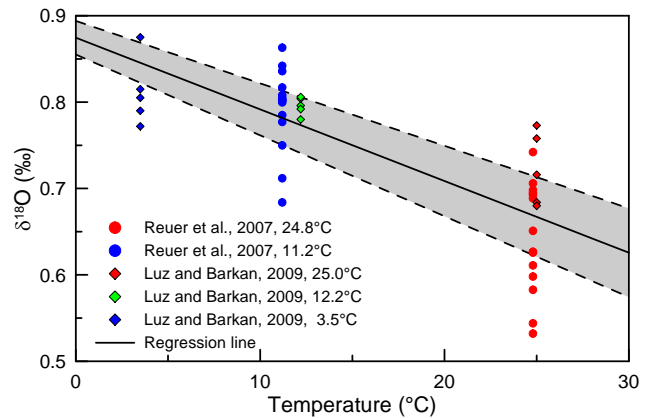


**Fig. A2**  $\delta^{18}\text{O}$  of dissolved  $\text{O}_2$  versus equilibrium temperature (Luz and Barkan, 2009; Reuer et al., 2007). The gray area represents the 1 sigma uncertainty for the regression line.

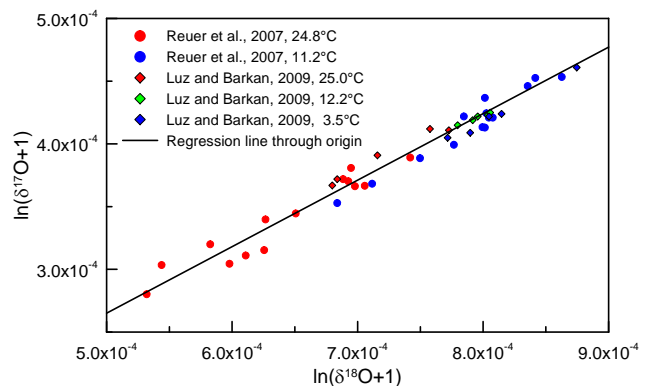


**Fig. A3**  $^{17}\text{O}$  vs.  $^{18}\text{O}$  of dissolved  $\text{O}_2$  (Luz and Barkan, 2009; Reuer et al., 2007).

## Appendix A

### Correlation between $^{17}\Delta$ and $\text{CO}_2$

For the correlation plot (Fig. A1), as for Fig. 1, the  $^{17}\Delta$  and  $\text{CO}_2$  data were interpolated and smoothed with a Gaussian filter with  $\sigma = 1.5$  ka. Where applicable, the data were weighted relative to the precision of the individual datum.

## Appendix B

### Equilibrium fractionation of dissolved $\text{O}_2$

Reuer et al. (2007) found a  $\lambda$  of 0.528 for dissolved  $\text{O}_2$  at equilibrium with  $\text{O}_2$  in the gas phase. They further found no significant temperature dependence of the  $^{17}\Delta$  of the dissolved  $\text{O}_2$ . Conflicting with these results Luz and Barkan (2009) found a significant temperature dependence



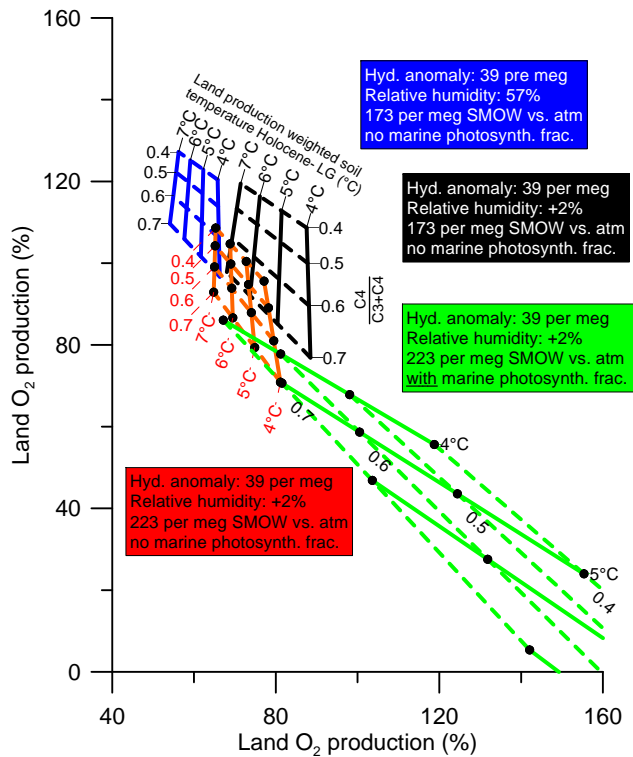


**Fig. A4** Effect of initializing the calculations with a  $^{17}\Delta$  modern ocean water vs. modern atmosphere of 173 and 223 per meg, respectively (Barkan and Luz, 2011), and allowing fractionation during marine photosynthesis (Luz and Barkan, 2011) for a LGM situation (Table 4). In blue the standard case with 173 per meg modern ocean water vs. modern atmosphere. For all other calculations the relative humidity was increased by 2% with respect to the initialization value. The calculations were made with 173 per meg modern ocean water vs. modern atmosphere in black, and 223 per meg in red and green. Marine photosynthetic fractionation was set to 4‰ in  $\delta^{18}\text{O}$  ( $\lambda$  of 0.524) for the green case only.

of the  $^{17}\Delta$  of the dissolved  $\text{O}_2$ , which results in a temperature dependent  $\lambda$ . We recalculate  $\lambda$  as a single value from all available data and obtain  $\lambda = 0.5284 \pm 0.0017$  (Fig. A2).

On the other hand, both datasets show a temperature dependence of the  $\delta^{18}\text{O}$  in the dissolved  $\text{O}_2$ . From the combined dataset we calculate a temperature dependent fractionation factor of  $\varepsilon_*$  (‰) =  $0.8746 - 0.0083 \cdot T(^{\circ}\text{C})$  for  $^{18}\text{O}$  (Fig. A3).

## Appendix C

### Distribution of C3 and C4 plants

Estimating values for the relative abundance of C3 and C4 plants is essential for our calculations. In the following we summarize our knowledge about the distribution of C4

plants, thereby justifying the range of last glacial C4 to C3 partitioning used in our calculations.

Estimates of the C4 fraction, calculated prognostically using two biosphere models driven by GCMs, vary widely. François et al. (1998) give 0.39 for the fraction of LGM productivity associated with C4 plants, compared with 0.28 for the modern (expressed as net carbon production). On the other hand, Landais et al. (2007) calculate the contribution of C4 plants to the total carbon GPP with the ORCHIDEE model to be 0.66 for the LGM and 0.22 for modern conditions (Landais, personal correspondence, 2008). Other modeling studies simulate properties of LGM vegetation that allow us to put rough limits on the fraction of land photosynthesis that they attribute to C4 plants. Beerling and Woodward (2001) use a coupled vegetation–biochemistry model, which includes mechanistic models of the C3 and C4 pathways, in the context of the UGAMP and NCAR paleoclimate simulations. From their simulations, we estimate that the modern ratio of land C4/(C3 + C4) production is 0.32 and was 0.4 (NCAR)–0.5 (UGAMP) at the LGM. These numbers are derived using ratios of carbon NPP/phytomass from François et al. (1998) to scale Beerling and Woodward’s (2001) estimates of biomass to NPP. The estimates for the LGM C4 fraction span a range from 1.4 to 3 times their respective modern extent. However, we argue that the increase of C4 plants was probably rather at the lower end of the above estimates.

An indicator of the fractional production by C3 and C4 plants is the extent of the area occupied by these plant functional types. Collatz et al. (1998) estimate that C4 currently occupies  $\sim 43\%$  of total land area, and increased only moderately to 53% during the LGM. This estimate is based on the physiological responses of C3 and C4 plants. The loss of forests in places where the ice sheets expand during the glacial seem to have been compensated for to some extent south of the ice sheets. According to summaries from pollen studies for the LGM, North America was largely forested south of the ice sheets, with scrub and woodland covering much of Mexico. Over South America the reconstruction of Ray and Adams (2001) shows grassland and desert over much of the continent but forest covering most of the equatorial land. Also, Colinvaux and De Oliveira (2000, and elsewhere) have argued vigorously that the Amazon was forested during the LGM.

Further studies of carbon isotopes in samples of regional significance give evidence for C3/C4 abundance during the LGM. Even at the LGM, C3 plants accounted for an important part of grassland communities in Texas and much of Africa (Koch et al., 2004; Scott, 2002; Rommerskirchen et al., 2006). On the Chinese Loess Plateau,  $\delta^{13}\text{C}$  of LGM organic matter actually decreased relative to modern (Gu et al., 2003). The authors interpreted this result as indicating that lowered temperatures overshadowed lower  $\text{CO}_2$ , thereby promoting C3 over C4.



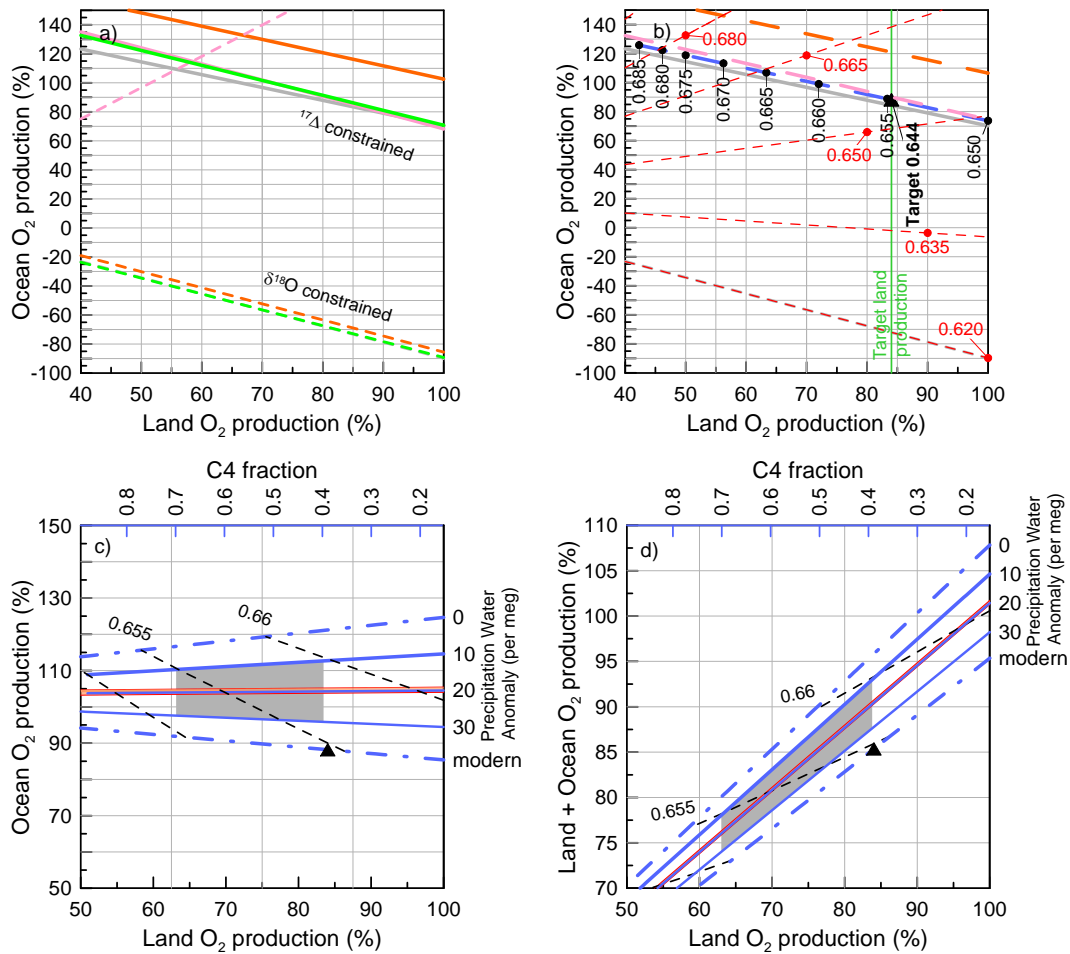


**Fig. A5** Similar to Fig. 3 in the main text. Plots of ocean O<sub>2</sub> production vs. land O<sub>2</sub> production (a–c) and total O<sub>2</sub> production vs. land O<sub>2</sub> production (d) for the Last Glacial Maximum default scenario (see Table 4). The lines and areas indicate allowable values as constrained by the  $\delta^{18}\text{O}$  and  $^{17}\Delta$  of paleo-atmospheric O<sub>2</sub> relative to the modern (100 %) production. (a) Gray dashed and solid line: solutions that satisfy  $\delta^{18}\text{O}$  atm and  $^{17}\Delta$ , respectively, assuming modern humidity and a hydrological anomaly similar to modern. For a  $^{17}\Delta$  ocean water vs. atmosphere of 223 per meg and a 4.0 ‰  $\delta^{18}\text{O}$  marine photosynthetic enrichment ( $\lambda$  0.524) with respect to seawater in the surface ocean. The orange lines are calculated for identical conditions but with a 20 % increased stratospheric flux. Pink lines are for a  $^{17}\Delta$  ocean water vs. atmosphere of 223 per meg and no photosynthetic enrichment. (b) Solutions of (a) in gray. Increasing the relative humidity (black dots and associated labels; blue line for the gray scenario in (a)) drives the intercept of  $^{17}\Delta$  and  $\delta^{18}\text{O}$  towards the target value for land productivity (see text for details). The light dashed red lines give solutions for  $\delta^{18}\text{O}$  with increasing relative humidity (for the gray scenario in (a)). The  $^{17}\Delta$  line is hardly affected by variable relative humidity. (c) and (d) Again, for a  $^{17}\Delta$  ocean water vs. atmosphere of 223 per meg and a 4.0 ‰  $\delta^{18}\text{O}$  marine photosynthetic enrichment ( $\lambda$  0.524) with respect to seawater in the surface ocean, the value for land carbon productivity is locked. Therefore, the land O<sub>2</sub> production is inversely proportional to the C4 contribution (top axis). We show solutions for precipitation anomalies from 0 to 40 per meg and soil temperature 5 °C lower than modern. The lines in red represents solutions with soil temperatures 4–7 °C lower than modern and a precipitation  $^{17}\Delta$  anomaly of 20 per meg lower than modern. Black dashed lines show isolines of global GPP-weighted humidity. The gray area represents solutions we favor. Black triangles show the target value of (b).

For the last piece of evidence we turn to the  $\delta^{13}\text{C}$  signature of atmospheric CO<sub>2</sub>. Compared to the last millennium,  $\delta^{13}\text{C}$  was depleted by about 0.3 ‰ during the Last Glacial Maximum (Leuenberger et al., 1992). On the long-term time scale, this shift has to be explained by (1) the transfer of carbon from the terrestrial reservoir (including soil carbon) to the ocean/atmosphere carbon pool and (2) changes in the parti-

tioning of C3 and C4 plants in the terrestrial biosphere. Both the anticipated increase in C4 plants and a reduced terrestrial biosphere during the glacial lead to lighter  $\delta^{13}\text{C}$  in the glacial atmosphere. Estimates for the Last Glacial Maximum terrestrial biomass (including soil carbon) are in the range of 48–58 % of the pre-industrial value of about 2000 GtC (Tables 5 and 7, Otto et al., 2002). This reduction is enough to

explain the observed  $\delta^{13}\text{C}$  depletion, requiring no change in the C4 partition. We therefore believe that C4 partition was only moderately increased in the glacial. Our calculation is based on an atmosphere/ocean reservoir of 40 000 GtC and a Holocene C4 partition of 27.5%. For  $\delta^{13}\text{C}$  of C3 and C4 plants, we take  $-27\%$  and  $-12\%$ , respectively.

All evidence points towards a low to moderate increase in C4 biomass during the glacial. While we calculate past GPP invoking a glacial C4 partition of 40–70%, we clearly favor values at the lower end of this range.

**Supplementary material related to this article is available online at: <http://www.clim-past.net/8/1509/2012/cp-8-1509-2012-supplement.zip>.**

*Acknowledgements.* This work was supported by the US National Science Foundation. We thank Peter Langen for performing runs with the NCAR model for relative humidity. This work has benefited from discussions with Boaz Luz, Amaëlle Landais, Renato Winkler, and Susanne von Caemmerer. Any errors are our responsibility alone.

Edited by: D. Fleitmann

## References

- Angert, A., Barkan, E., Barnett, B., Brugnoli, E., Davidson, E. A., Fessenden, J., Maneepong, S., Panapitukkul, N., Randerson, J. T., Savage, K., Yakir, D., and Luz, B.: Contribution of soil respiration in tropical, temperate, and boreal forests to the  $^{18}\text{O}$  enrichment of atmospheric  $\text{O}_2$ , *Global Biogeochem. Cy.*, 17, 1089, doi:10.1029/2002GB001933, 2003a.
- Angert, A., Rachmilevitch, S., Barkan, E., and Luz, B.: Effects of photorespiration, the cytochrome pathway, and the alternative pathway on the triple isotopic composition of atmospheric  $\text{O}_2$ , *Global Biogeochem. Cy.*, 17, 1030, doi:10.1029/2002GB001933, 2003b.
- Appenzeller, C., Holton, J. R., and Rosenlof, K. H.: Seasonal variation of mass transport across the tropopause, *J. Geophys. Res.*, 101, 15071–15078, 1996.
- Barkan, E. and Luz, B.: High precision measurements of  $^{17}\text{O}/^{16}\text{O}$  and  $^{18}\text{O}/^{16}\text{O}$  in  $\text{H}_2\text{O}$ , *Rapid Commun. Mass Sp.*, 19, 3737–3742, 2005.
- Barkan, E. and Luz, B.: Diffusivity fractionations of  $\text{H}_2^{16}\text{O}/\text{H}_2^{17}\text{O}$  and  $\text{H}_2^{16}\text{O}/\text{H}_2^{18}\text{O}$  in air and their implications for isotope hydrology, *Rapid Commun. Mass Sp.*, 21, 2999–3005, 2007.
- Barkan, E. and Luz, B.: The relationships among the three stable isotopes of oxygen in air, seawater and marine photosynthesis, *Rapid Commun. Mass Sp.*, 25, 2367–2369, doi:10.1002/rcm.5125, 2011.
- Beerling, D. J. and Woodward, F. I.: *Vegetation and the terrestrial carbon cycle: Modelling the first 400 million years*, Cambridge University Press, Cambridge, UK, New York, NY, 405 pp., 2001.
- Behrenfeld, M. J. and Falkowski, P. G.: Photosynthetic rates derived from satellite-based chlorophyll concentration, *Limnol. Oceanogr.*, 42, 1–20, 1997.
- Bender, M. L.: Orbital tuning chronology for the Vostok climate record supported by trapped gas composition, *Earth Planet. Sc. Lett.*, 204, 275–289, 2002.
- Bender, M. L., Sowers, T., and Labeyrie, L.: The Dole effect and its variations during the last 130,000 years as measured in the Vostok ice core, *Global Biogeochem. Cy.*, 8, 363–376, 1994.
- Bender, M. L., Dickson, M. L., and Orchardo, J.: Net and gross production in the Ross Sea as determined by incubation experiments and dissolved  $\text{O}_2$  studies, *Deep-Sea Res. Pt II*, 47, 3141–3158, 2000.
- Blunier, T. and Brook, E. J.: Timing of millennial-scale climate change in Antarctica and Greenland during the last glacial period, *Science*, 291, 109–112, doi:10.1126/science.291.5501.109, 2001.
- Blunier, T., Barnett, B., Bender, M. L., and Hendricks, M. B.: Biological oxygen productivity during the last 60,000 years from triple oxygen isotope measurements, *Global Biogeochem. Cy.*, 16, 3, doi:10.1029/2001GB001460, 2002.
- Boering, K. A., Jackson, T., Hoag, K. J., Cole, A. S., Perri, M. J., Thieme, M., and Atlas, E.: Observations of the anomalous oxygen isotopic composition of carbon dioxide in the lower stratosphere and the flux of the anomaly to the troposphere, *Geophys. Res. Lett.*, 31, L03109, doi:10.1029/2003GL018451, 2004.
- Bopp, L., Kohfeld, K. E., Le Quere, C., and Aumont, O.: Dust impact on marine biota and atmospheric  $\text{CO}_2$  during glacial periods, *Paleoceanography*, 18, 1046, doi:10.1029/2002pa000810, 2003.
- Bottinga, Y. and Craig, H.: Oxygen isotope fractionation between  $\text{CO}_2$  and water, and the isotopic composition of marine atmospheric  $\text{CO}_2$ , *Earth Planet. Sc. Lett.*, 5, 285–295, 1969.
- Brook, E. J., White, J. W. C., Schilla, A. S. M., Bender, M. L., Barnett, B., Severinghaus, J. P., Taylor, K. C., Alley, R. B., and Steig, E. J.: Timing of millennial-scale climate change at Siple Dome, West Antarctica, during the last glacial period, *Quaternary Sci. Rev.*, 24, 1333–1343, 2005.
- Claustre, H., Huot, Y., Obernosterer, I., Gentili, B., Tailliez, D., and Lewis, M.: Gross community production and metabolic balance in the South Pacific Gyre, using a non-invasive bio-optical method, *Biogeosciences*, 5, 463–474, doi:10.5194/bg-5-463-2008, 2008.
- Colinvaux, P. A. and De Oliveira, P. E.: Palaeoecology and climate of the Amazon basin during the last glacial cycle, *J. Quaternary Sci.*, 15, 347–356, 2000.
- Collatz, G. J., Berry, J. A., and Clark, J. S.: Effects of climate and atmospheric  $\text{CO}_2$  partial pressure on the global distribution of C4 grasses: Present, past and future, *Oecologia*, 114, 441–454, 1998.
- Denman, K. L., Brasseur, G., Chidthaisong, A., Ciais, P., Cox, P. M., Dickinson, R. E., Hauglustaine, D., Heinze, C., Holland, E., Jacob, D., Lohmann, U., Ramachandran, S., Dias, P. L. d. S., Wofsy, S. C., and Zhang, X.: Couplings between changes in the climate system and biogeochemistry, in: *Climate Change 2007: The Physical Science Basis. Contribution of Working Group I to the Fourth Assessment Report of the Intergovernmental Panel on Climate Change*, edited by: Solomon, S., Qin, D., Manning, M., Chen, Z., Marquis, M., Averyt, K. B., Tignor, M., and Miller, H. L., Cambridge University Press, Cambridge, United Kingdom and New York, NY, USA, 2007.

- Ehhalt, D., Prather, M., Dentener, F., Derwent, R., Dlugokencky, E., Holland, E., Isaksen, I., Katima, J., Kirchhoff, V., Matson, P., Midgley, P., and Wang, M.: Atmospheric chemistry and greenhouse gases, in: *Climate change 2001: The scientific basis. Contribution of working group I to the third assessment report of the intergovernmental panel on climate change*, edited by: Houghton, J. T., Ding, Y., Griggs, D. J., Noguer, M., van der Linden, P. J., Dai, X., Maskell, K., and Johnson, C. A., Cambridge University Press, Cambridge [etc.], 881 S., 2001.
- Eisenstadt, D., Barkan, E., Luz, B., and Kaplan, A.: Enrichment of oxygen heavy isotopes during photosynthesis in phytoplankton, *Photosynth. Res.*, 103, 97–103, doi:10.1007/s11120-009-9518-z, 2010.
- Emerson, S., Quay, P. D., Stump, C., Wilbur, D., and Schudlich, R.: Chemical tracers of productivity and respiration in the subtropical Pacific-ocean, *J. Geophys. Res.-Oceans*, 100, 15873–15887, 1995.
- Farquhar, G. D., Hubick, K. T., Condon, A. G., and Richards, R. A.: Carbon isotope fractionation and plant water-use efficiency, in: *Stable isotopes in ecological research*, edited by: Rundel, P. W., Ehleringer, J. R., and Nagy, K. A., Springer Verlag, New York, Berlin, Heidelberg, 21–40, 1989.
- Farquhar, G. D., Lloyd, J., Taylor, J. A., Flanagan, L. B., Syvertsen, J. P., Hubick, K. T., Wong, S. C., and Ehleringer, J. R.: Vegetation effects on the isotope composition of oxygen in atmospheric CO<sub>2</sub>, *Nature*, 363, 439–442, 1993.
- Field, C. B., Behrenfeld, M. J., Randerson, J. T., and Falkowski, P.: Primary production of the biosphere: Integrating terrestrial and oceanic components, *Science*, 281, 237–240, 1998.
- François, L. M., Delire, C., Warnant, P., and Munhoven, G.: Modelling the glacial-interglacial changes in the continental biosphere, *Global Planet. Change*, 17, 37–52, 1998.
- Gu, Z. Y., Liu, Q., Xu, B., Han, J. M., Yang, S. L., Ding, Z. L., and Liu, T. S.: Climate as the dominant control on C-3 and C-4 plant abundance in the loess plateau: Organic carbon isotope evidence from the last glacial-interglacial loess-soil sequences, *Chinese Science Bull.*, 48, 1271–1276, 2003.
- Guy, R. D., Berry, J. A., Fogel, M. L., Turpin, D. H., and Weger, H. G.: Fractionation of the stable isotopes of oxygen during respiration by plants - the basis of a new technique to estimate partitioning to the alternative path, in: *Molecular, biochemical and physiological aspects of plant respiration*, edited by: Lambers, H. and van der Plas, L. H. W., SPB Academic Publishing, The Hague, The Netherlands, 443–453, 1992.
- Guy, R. D., Fogel, M. L., and Berry, J. A.: Photosynthetic fractionation of the stable isotopes of oxygen and carbon, *Plant. Physiol.*, 101, 37–48, 1993.
- Helman, Y., Barkan, E., Eisenstadt, D., Luz, B., and Kaplan, A.: Fractionation of the three stable oxygen isotopes by oxygen-producing and oxygen-consuming reactions in photosynthetic organisms, *Plant. Physiol.*, 138, 2292–2298, doi:10.1104/pp.105.063768, 2005.
- Hendricks, M. B., Bender, M. L., and Barnett, B. A.: Net and gross O<sub>2</sub> production in the southern ocean from measurements of biological O<sub>2</sub> saturation and its triple isotope composition, *Deep-Sea Res. Pt I*, 51, 1541–1561, 2004.
- Hirsch, A. I., Michalak, A. M., Bruhwiler, L. M., Peters, W., Dlugokencky, E. J., and Tans, P. P.: Inverse modeling estimates of the global nitrous oxide surface flux from 1998–2001, *Global Biogeochem. Cy.*, 20, GB1008, doi:10.1029/2004GB002443, 2006.
- Hoefs, J.: *Stable isotope geochemistry*, 4th Edn., Springer, Berlin, New York, 201 pp., 1996.
- Hoffmann, G., Cuntz, M., Weber, C., Ciais, P., Friedlingstein, P., Heimann, M., Jouzel, J., Kaduk, J., Maier-Reimer, E., Seibt, U., and Six, K.: A model of the earth's Dole effect, *Global Biogeochem. Cy.*, 18, GB1008, doi:10.1029/2003GB002059, 2004.
- Jansen, E., Overpeck, J., Briffa, K. R., Duplessy, J. C., Joos, F., Masson-Delmotte, V., Olago, D., Otto-Bliesner, B., Peltier, W. R., Rahmstorf, S., Ramesh, R., Raynaud, D., Rind, D., Solomina, O., Villalba, R., and Zhang, D.: Palaeoclimate, in: *Climate change 2007: The physical science basis. Contribution of working group I to the fourth assessment report of the intergovernmental panel on climate change*, edited by: Solomon, S., Qin, D., Manning, M., Chen, Z., Marquis, M., Averyt, K. B., Tignor, M., and Miller, H. L., Cambridge University Press, Cambridge, United Kingdom and New York, NY, USA, 2007.
- Johnson, K. S., Riser, S. C., and Karl, D. M.: Nitrate supply from deep to near-surface waters of the north Pacific subtropical gyre, *Nature*, 465, 1062–1065, doi:10.1038/nature09170, 2010.
- Joos, F., Gerber, S., Prentice, I. C., Otto-Bliesner, B. L., and Valdes, P. J.: Transient simulations of holocene atmospheric carbon dioxide and terrestrial carbon since the last glacial maximum, *Global Biogeochem. Cy.*, 18, GB2002, doi:10.1029/2003GB002156, 2004.
- Jouzel, J., Hoffmann, G., Koster, R. D., and Masson, V.: Water isotopes in precipitation: Data/model comparison for present-day and past climates, *Quaternary Sci. Rev.*, 19, 363–379, 2000.
- Keeling, R. F.: Development of an interferometric oxygen analyzer for precise measurement of the atmospheric O<sub>2</sub> mole fraction, *The Division of Applied Sciences, Harvard University, Cambridge, Massachusetts*, 178 pp., 1988.
- Kiehl, J. T., Hack, J. J., Bonan, G. B., Boville, B. A., Williamson, D. L., and Rasch, P. J.: The national center for atmospheric research community climate model: CCM3, *J. Climate*, 11, 1131–1149, 1998.
- Koch, P. L., Duffenbaugh, N. S., and Hoppe, K. A.: The effects of late quaternary climate and pCO<sub>2</sub> change on C-4 plant abundance in the south-central United States, *Paleogeogr. Paleoclimatol.*, 207, 331–357, 2004.
- Kohfeld, K. E., Le Quere, C., Harrison, S. P., and Anderson, R. F.: Role of marine biology in glacial-interglacial CO<sub>2</sub> cycles, *Science*, 308, 74–78, 2005.
- Lämmerzahl, P., Röckmann, T., Brenninkmeijer, C. A. M., Krankowsky, D., and Mauersberger, K.: Oxygen isotope composition of stratospheric carbon dioxide, *Geophys. Res. Lett.*, 29, 12, doi:10.1029/2001GL014343, 2002.
- Landais, A., Barkan, E., Yakir, D., and Luz, B.: The triple isotopic composition of oxygen in leaf water, *Geochim. Cosmochim. Acta.*, 70, 4105–4115, 2006.
- Landais, A., Lathiere, J., Barkan, E., and Luz, B.: Reconsidering the change in global biosphere productivity between the last glacial maximum and present day from the triple oxygen isotopic composition of air trapped in ice cores, *Global Biogeochem. Cy.*, 21, GB1025, doi:10.1029/2006GB002739, 2007.
- Landais, A., Barkan, E., and Luz, B.: Record of delta δ<sup>18</sup>O and <sup>17</sup>O-excess in ice from Vostok Antarctica during the last 150,000 years, *Geophys. Res. Lett.*, 35, L02709, doi:10.1029/2007GL032096, 2008.

- Leuenberger, M., Siegenthaler, U., and Langway, C. C.: Carbon isotope composition of atmospheric CO<sub>2</sub> during the last ice age from an Antarctic ice core, *Nature*, 357, 488–490, 1992.
- Li, F. Y., Ramaswamy, V., Ginoux, P., Broccoli, A. J., Delworth, T., and Zeng, F. R.: Toward understanding the dust deposition in Antarctica during the last glacial maximum: Sensitivity studies on plausible causes, *J. Geophys. Res.-Atmos.*, 115, D24120, doi:10.1029/2010jd014791, 2010.
- Li, W. J. and Meijer, H. A. J.: The use of electrolysis for accurate  $\delta^{17}\text{O}$  and  $\delta^{18}\text{O}$  isotope measurements in water, *Isot. Environ. Health S*, 34, 349–369, 1998.
- Lüthi, D., Le Floch, M., Bereiter, B., Blunier, T., Barnola, J.-M., Siegenthaler, U., Raynaud, D., Jouzel, J., Fischer, H., Kawamura, K., and Stocker, T. F.: High-resolution carbon dioxide concentration record 650,000–800,000 years before present, *Nature*, 453, 379–382, 2008.
- Luz, B. and Barkan, E.: The isotopic ratios  $^{17}\text{O}/^{16}\text{O}$  and  $^{18}\text{O}/^{16}\text{O}$  in molecular oxygen and their significance in biogeochemistry, *Geochim. Cosmochim. Ac.*, 69, 1099–1110, doi:10.1016/j.gca.2004.09.001, 2005.
- Luz, B. and Barkan, E.: Net and gross oxygen production from O<sub>2</sub>/Ar,  $^{17}\text{O}/^{16}\text{O}$  and  $^{18}\text{O}/^{16}\text{O}$  ratios, *Aquatic Microbial Ecology*, 56, 133–145, doi:10.3354/ame01296, 2009.
- Luz, B. and Barkan, E.: The isotopic composition of atmospheric oxygen, *Global Biogeochem. Cy.*, 25, GB3001, doi:10.1029/2010gb003883, 2011.
- Luz, B., Barkan, E., Bender, M. L., Thiemens, M. H., and Boering, K. A.: Triple-isotope composition of atmospheric oxygen as a tracer of biosphere productivity, *Nature*, 400, 547–550, 1999.
- Manning, A. C. and Keeling, R. F.: Global oceanic and land biotic carbon sinks from the scripps atmospheric oxygen flask sampling network, *Tellus B*, 58, 95–116, 2006.
- Meese, D. A., Alley, R. B., Fiacco, R. J., Germani, M. S., Gow, A. J., Grootes, P. M., Illing, M., Mayewski, P. A., Morrison, M. C., Ram, M., Taylor, K. C., Yang, Q., and Zielinski, G. A.: Preliminary depth-agescale of the GISP2 ice core, Special CRREL Report, 94-1, US, 1994.
- Miller, M. F.: Isotopic fractionation and the quantification of  $^{17}\text{O}$  anomalies in the oxygen three-isotope system: An appraisal and geochemical significance, *Geochim. Cosmochim. Ac.*, 66, 1881–1889, 2002.
- Otto, D., Rasse, D., Kaplan, J., Warnant, P., and Francois, L.: Biospheric carbon stocks reconstructed at the last glacial maximum: Comparison between general circulation models using prescribed and computed sea surface temperatures, *Global Planet. Change*, 33, 117–138, 2002.
- Petit, J. R., Jouzel, J., Raynaud, D., Barkov, N. I., Barnola, J. M., Basile, I., Bender, M., Chappellaz, J., Davis, M., Delaygue, G., Delmotte, M., Kotlyakov, V. M., Legrand, M., Lipenkov, V. Y., Lorius, C., Pepin, L., Ritz, C., Saltzman, E., and Stevenard, M.: Climate and atmospheric history of the past 420,000 years from the Vostok ice core, Antarctica, *Nature*, 399, 429–436, 1999.
- Plumb, R. A. and Ko, M. K. W.: Interrelationships between mixing ratios of long lived stratospheric constituents, *J. Geophys. Res.-Atmos.*, 97, 10145–10156, 1992.
- Quay, P. D., Emerson, S., Wilbur, D. O., Stump, C., and Knox, M.: The  $\delta^{18}\text{O}$  of dissolved O<sub>2</sub> in the surface waters of the sub-arctic pacific - a tracer of biological productivity, *J. Geophys. Res.-Oceans*, 98, 8447–8458, 1993.
- Ray, N. and Adams, J. M.: A GIS-based vegetation map of the world at the last glacial maximum (25,000–15,000 BP), *Internet Archaeology*, 11, available at: <http://intarch.ac.uk/journal/issue11/rayadams.toc.html>, 2001.
- Reuer, M. K., Barnett, B. A., Bender, M. L., Falkowski, P. G., and Hendricks, M. B.: New estimates of southern ocean biological production rates from O<sub>2</sub>/Ar ratios and the triple isotope composition of O<sub>2</sub>, *Deep-Sea Res. Pt I*, 54, 951–974, 2007.
- Ribas-Carbo, M., Robinson, S. A., Gonzalez-Meler, M. A., Lennon, A. M., Giles, L., Siedow, J. N., and Berry, J. A.: Effects of light on respiration and oxygen isotope fractionation in soybean cotyledons, *Plant Cell Environ.*, 23, 983–989, doi:10.1046/j.1365-3040.2000.00607.x, 2000.
- Rommerskirchen, F., Eglinton, G., Dupont, L., and Rullkotter, J.: Glacial/interglacial changes in southern africa: Compound-specific  $\delta^{13}\text{C}$  land plant biomarker and pollen records from southeast atlantic continental margin sediments, *Geochem. Geophys. Geosyst.*, 7, Q08010, doi:10.1029/2005GC001223, 2006.
- Schlesinger, W. H. and Andrews, J. A.: Soil respiration and the global carbon cycle, *Biogeochemistry*, 48, 7–20, 2000.
- Schrag, D. P., Adkins, J. F., McIntyre, K., Alexander, J. L., Hodell, D. A., Charles, C. D., and McManus, J. F.: The oxygen isotopic composition of seawater during the last glacial maximum, *Quaternary Sci. Rev.*, 21, 331–342, 2002.
- Scott, L.: Grassland development under glacial and interglacial conditions in southern africa: Review of pollen, phytolith and isotope evidence, *Paleogeogr. Paleoclimatol. Paleocol.*, 177, 47–57, 2002.
- Shackleton, N. J.: The 100'000-year ice-age cycle identified and found to lag temperature, carbon dioxide and orbital eccentricity, *Science*, 289, 1897–1902, 2000.
- Smythe-Wright, D., Boswell, S. M., Breithaupt, P., Davidson, R. D., Dimmer, C. H., and Diaz, L. B. E.: Methyl iodide production in the ocean: Implications for climate change, *Global Biogeochem. Cy.*, 20, GB3003, doi:10.1029/2005GB002642, 2006.
- Steemann Nielsen, E.: Measurement of the production of organic matter in the sea by means of carbon-14, *Nature*, 167, 684–685, doi:10.1038/167684b0, 1951.
- Suwa, M. and Bender, M. L.: Chronology of the Vostok ice core constrained by O<sub>2</sub>/N<sub>2</sub> ratios of occluded air, and its implication for the Vostok climate records, *Quaternary Sci. Rev.*, 27, 1093–1106, 2008.
- Thiemens, M. H., Jackson, T., Zipf, E. C., Erdman, P. W., and Vanegmond, C.: Carbon-dioxide and oxygen-isotope anomalies in the mesosphere and stratosphere, *Science*, 270, 969–972, 1995.
- von Caemmerer, S. and Farquhar, G. D.: Some relationships between the biochemistry of photosynthesis and the gas-exchange of leaves, *Planta*, 153, 376–387, 1981.
- Winkler, R., Landais, A., Sodemann, H., Dümbgen, L., Prié, F., Masson-Delmotte, V., Stenni, B., and Jouzel, J.: Deglaciation records of  $^{17}\text{O}$ -excess in East Antarctica: reliable reconstruction of oceanic normalized relative humidity from coastal sites, *Clim. Past*, 8, 1–16, doi:10.5194/cp-8-1-2012, 2012.
- Yung, Y. L., Lee, A. Y. T., Irion, F. W., DeMore, W. B., and Wen, J.: Carbon dioxide in the atmosphere: Isotopic exchange with ozone and its use as a tracer in the middle atmosphere, *J. Geophys. Res.-Atmos.*, 102, 10857–10866, 1997.